AD-A165 993 CSC METEOR BURST MODEL ENHANCEMENT TEST REPORT(U) 1/1
COMPUTER SCIENCES CORP FALLS CHURCH VA SYSTEMS DIV
W STEFFANCIN ET AL. FEB 86 DCA100-84-C-0030

UNCLASSIFIED F/G 17/2.1 NL

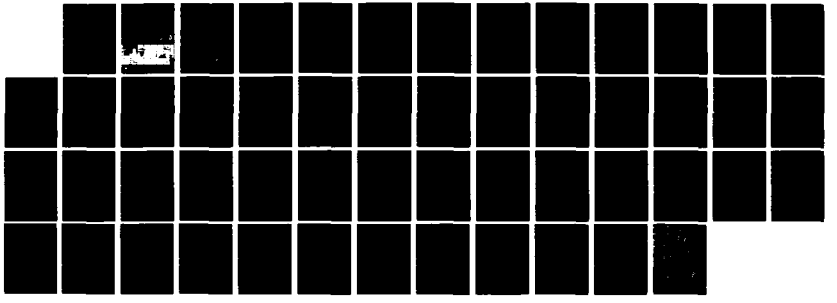

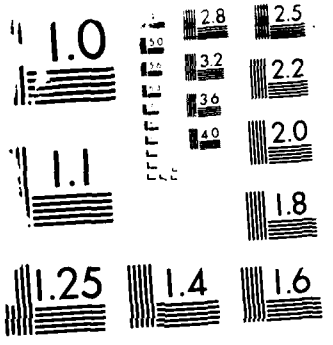

MICROCOPY RESOLUTION TEST CHART

CSC METEOR BURST MODEL ENHANCEMENT TEST REPORT

Prepared for
DEFENSE COMMUNICATIONS AGENCY
Washington, D.C. 20305

Under
CONTRACT DCA100-84-C-0030
TASK ORDER 7-85, SUBTASK 1

FEBRUARY 1986

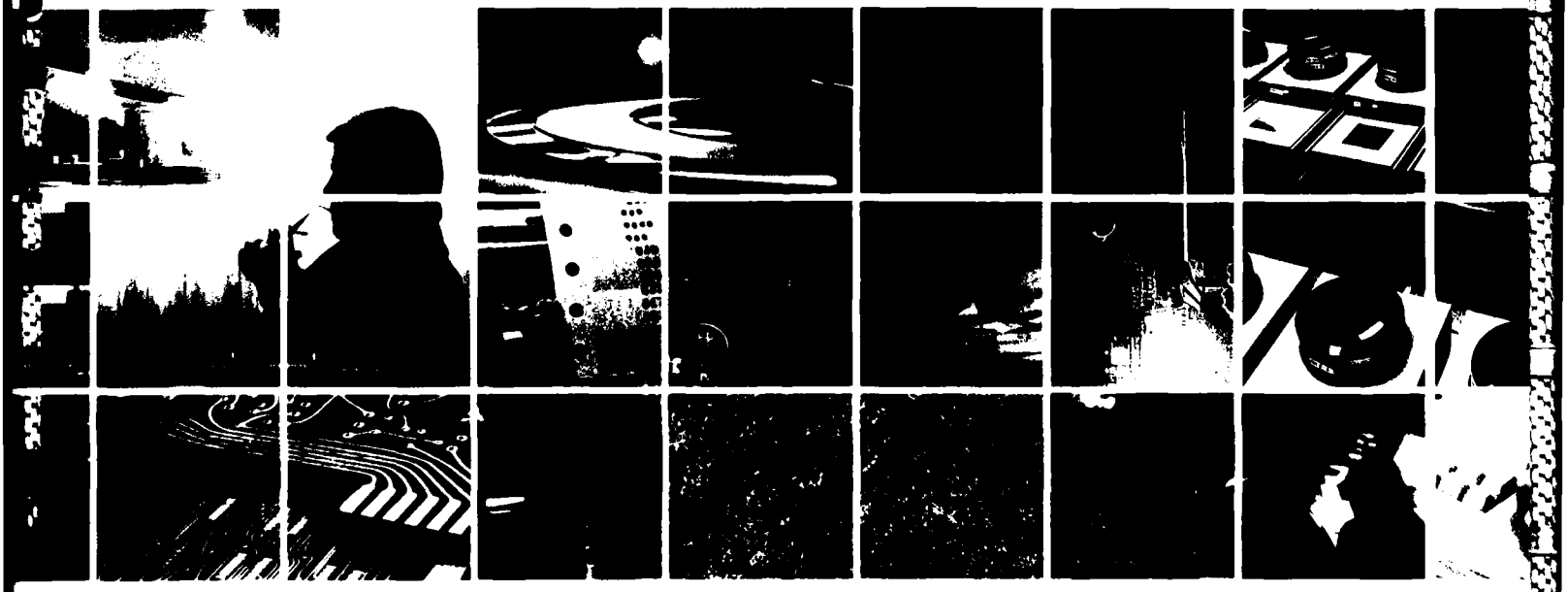

CSC
COMPUTER SCIENCES CORPORATION
SYSTEMS DIVISION

CSC METEOR BURST MODEL ENHANCEMENT TEST REPORT

Prepared for
DEFENSE COMMUNICATIONS AGENCY
Washington, D.C. 20305

Under
CONTRACT DCA100-84-C-0030
TASK ORDER 7-85, SUBTASK 1

FEBRUARY 1986

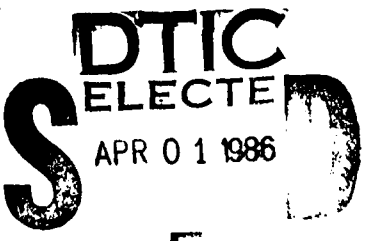

CSC
COMPUTER SCIENCES CORPORATION
SYSTEMS DIVISION
6565 Arlington Boulevard • Falls Chu[illegible], VA 22046

UNCLASSIFIED

SECURITY CLASSIFICATION OF THIS PAGE

AD-A165 993

REPORT DOCUMENTATION PAGE

1a. REPORT SECURITY CLASSIFICATION: UNCLASSIFIED	1b. RESTRICTIVE MARKINGS: None
2a. SECURITY CLASSIFICATION AUTHORITY: DD254	3. DISTRIBUTION/AVAILABILITY OF REPORT: Unlimited
2b. DECLASSIFICATION/DOWNGRADING SCHEDULE	
4. PERFORMING ORGANIZATION REPORT NUMBER(S)	5. MONITORING ORGANIZATION REPORT NUMBER(S)
6a. NAME OF PERFORMING ORGANIZATION: Computer Sciences Corp. (6b. OFFICE SYMBOL (If applicable))	7a. NAME OF MONITORING ORGANIZATION: Defense Communications Agency
6c. ADDRESS (City, State and ZIP Code): 6565 Arlington Boulevard, Falls Church, VA 22046	7b. ADDRESS (City, State and ZIP Code): Defense Comm. Engineering Center, 1860 Wiehle Avenue, Reston, VA 22090
8a. NAME OF FUNDING/SPONSORING ORGANIZATION (8b. OFFICE SYMBOL (If applicable))	9. PROCUREMENT INSTRUMENT IDENTIFICATION NUMBER: DCA100-84-C-0030
8c. ADDRESS (City, State and ZIP Code)	10. SOURCE OF FUNDING NOS: PROGRAM ELEMENT NO. / PROJECT NO. / TASK NO. / WORK UNIT NO.
11. TITLE (Include Security Classification): CSC Meteor Burst Model Enhancement Test Report (U)	
12. PERSONAL AUTHOR(S): W. Steffancin, D. Brown	
13a. TYPE OF REPORT: Interim	13b. TIME COVERED: FROM Apr 85 TO Feb 86
14. DATE OF REPORT (Yr., Mo., Day): 1986 February	15. PAGE COUNT: 49
16. SUPPLEMENTARY NOTATION	

17. COSATI CODES		
FIELD	GROUP	SUB. GR.

18. SUBJECT TERMS (Continue on reverse if necessary and identify by block number)

Meteor Burst Communications, Overdense bursts, Absorption (PCA), Shower meteors, Airborne terminals, Physical modeling

19. ABSTRACT (Continue on reverse if necessary and identify by block number)

This report describes enhancements made to the CSC meteor burst model in 1985 and presents and analyzes the effects of the enhancements on model results. The enhancements made include the effects of: overdense bursts, transverse resonance, burst formation, atmospheric refraction, ionospheric absorption, shower meteors and the earth's gravitational effect on meteor radiants.

20. DISTRIBUTION/AVAILABILITY OF ABSTRACT: UNCLASSIFIED/UNLIMITED ☒ SAME AS RPT. ☐ DTIC USERS ☐	21. ABSTRACT SECURITY CLASSIFICATION: UNCLASSIFIED
22a. NAME OF RESPONSIBLE INDIVIDUAL: Mr. R. L. Rhodes	22b. TELEPHONE NUMBER (Include Area Code): (703) 437-2083 / 22c. OFFICE SYMBOL: R220

DD FORM 1473, 83 APR EDITION OF 1 JAN 73 IS OBSOLETE.

UNCLASSIFIED

SECURITY CLASSIFICATION OF THIS PAGE

TABLE OF CONTENTS

LIST OF ILLUSTRATIONS

LIST OF TABLES

SECTION 1 - INTRODUCTION

The goal of this Subtask 1 Report is to describe the results of testing certain enhancements to the CSC meteor burst propagation prediction model implemented under Task 7-85 of Contract DCA100-84-C-0030. Under Task 7-84 an analysis of the preexisting CSC meteor burst model concluded that a number of enhancements could be implemented to extend the model's capabilities and improve its accuracy. The enhancements deemed desirable include:

- Ionospheric Absorption Effects (e.g., Polar Cap Absorption)
- The Effect of Horizon Blockage, which varies with Azimuth
- Overdense Bursts and Transient/Resonance Effects
- Refraction in the Lower Atmosphere
- The Capability to Model Airborne Terminals
- The Earth's Gravitational Effects on Meteor Radiants.

To facilitate the implementation of these enhancements, a restructuring of the propagation model was undertaken. The code was converted from FORTRAN to Pascal to take advantage of user-defined ordinal types and structured types associated with Pascal. New data types were created to minimize subprocedure parameter lists and provide variables and data structures for new enhancements. The code conversion also facilitated making the user interface "user friendly." Furthermore, the propagation model was separated into input and simulation programs with the option to execute interactively or in batch mode at the user's discretion.

Other alterations to the model made under Task 7-85 include the removal of a forced seasonal variation of meteor rates, which has been found to be inappropriate. The antenna modeling routines

have been generalized to allow user-definable antennas by means of files of radiation pattern data. Additionally, certain routines at the heart of the model that are executed a large number of times per run have been recoded to reduce run time. The effects of those meteor showers that recur each year have been added to the model of background sporadic meteors.

Section 3 of this report describes the meteor burst links used to test the enhancements and presents results of runs with the preexisting model to be used as a baseline for enhancement testing. Section 4 analyzes the test results for each enhancement. A summary and conclusions are presented in Section 5.

SECTION 2 - REFERENCES

This CSC Meteor Burst Model Enhancement Test Report is supported by the following references:

1. "Some Algorithms for Modeling Meteor Burst Propagation Modeling (U)," Computer Sciences Corporation, Contract DCA100-84-C-0030, February 1985.

2. "CSC Meteor Burst Model - Users Manual," Computer Sciences Corporation, Contract DCA100-84-C-0030, February 1986.

3. "CSC Meteor Burst Model - Maintenance Manual," Computer Sciences Corporation, Contract DCA100-84-C-0030, February 1986.

4. "A Physical Meteor Burst Model and Some Significant Results for Communications System Design," D. W. Brown, IEEE Journal on Selected Areas in Communications, Vol. SAC-3, No. 5, September 1985.

SECTION 3 - DESCRIPTION OF BASELINE LINKS

Baseline computations using the preexisting meteor burst model were run to provide a basis for comparison for the enhanced meteor burst model as it was developed. A description of the links used in the baseline and comparison runs is given in Tables 3-1 and 3-2.

The Greenland link runs were based on days in February and April for which Rome Air Development Center (RADC) experimental data was available. Runs were made at 2-hour intervals from 0200 hrs to 2400 hrs.

Plots of the baseline outputs for meteor rate (useful bursts/hour), average burst length (burst length in seconds averaged over all bursts in a measurement interval), duty cycle (the fraction of time a burst is available), and cosmic noise versus time of day for the Greenland link for February are shown in Figure 3-1. Figure 3-2 shows the model outputs for a mid-April date.

Figure 3-3 shows baseline duty cycle on the SHAPE Technical Centre (STC) link for an early June date.

Table 3-1. Parameters Used to Model the RADC Meteor Burst Link in Greenland

Transmitter Location	66.98N 50.65W
Receiver Location	76.55N 67.85W
Path Length	1209.9 km
Relevant Frequency	45 MHz
Transmit Power	650 W
Transmit Antenna	One 6-element Yagi at 1.50 wavelengths
Receive Antenna	One 6-element Yagi at 1.50 wavelengths
Antenna Orientation	Great Circle and Horizontal
Polarization	Horizontal
Soil Conductivity	0.0001 mhos/m (assumed)
Soil Dielectric Constant	2.50 (assumed)
Receiver Noise Figure	1.30 dB
Receiver E_b/N_o at Threshold*	8.0 dB
Receiver Bandwidth	*30,000 Hz*

*Threshold implies a minimum tolerable level of performance as determined by the user (e.g. a Bit Error Rate of 1 in 10^4).

Table 3-2. Parameters Used to Model the STC Meteor Burst Circuit

Transmitter Location	43.1N 6.0E
Receiver Location	51.9N 4.5E
Path Length	985 km
Relevant Frequency	36.59 MHz
Transmit Power	400 Watts
Transmit Antenna	5-element Yagi at 2 wavelengths
Receive Antenna 1	5-element Yagi at 1.2 wavelengths
Receive Antenna 2	5-element Yagi at 2.6 wavelengths
Antenna Orientation	Great Circle and Horizontal
Polarization	Horizontal
Soil Conductivity	.002 mhos/m
Soil Dielectric Constant	10.0
Receiver Noise Figure	4.0 dB
Receiver Eb/No at Threshold	8.0 dB
Receiver Bandwidth	2000 Hz

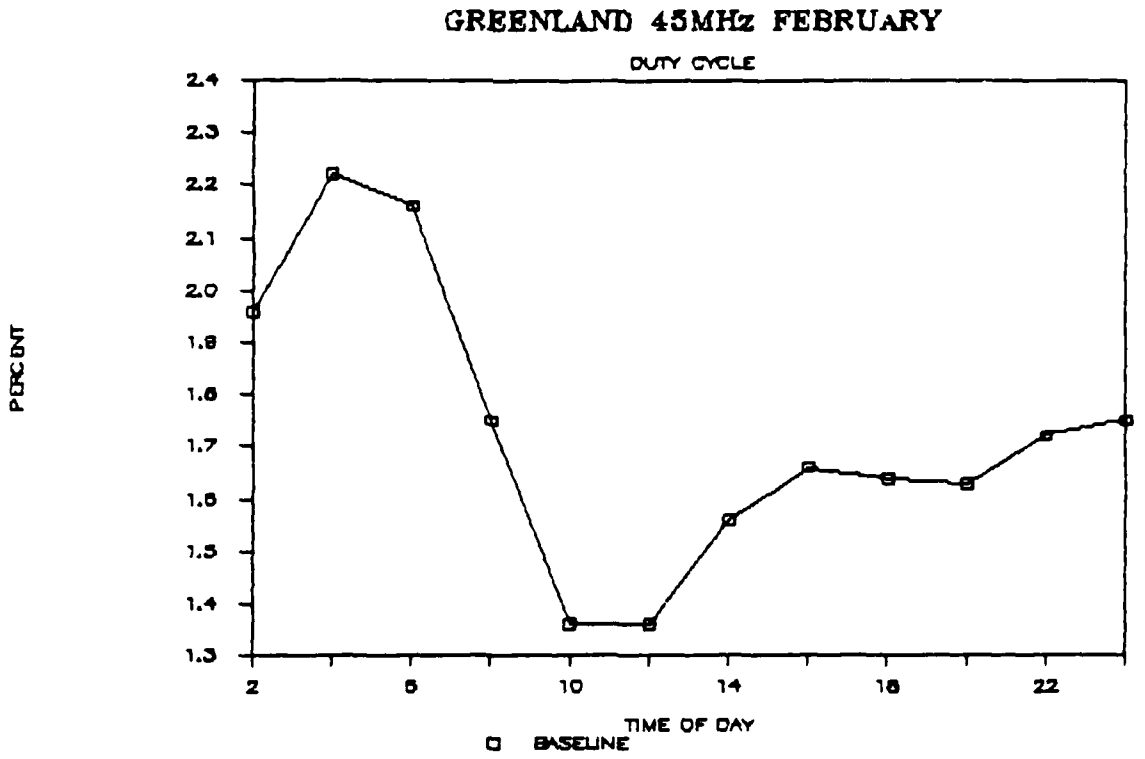

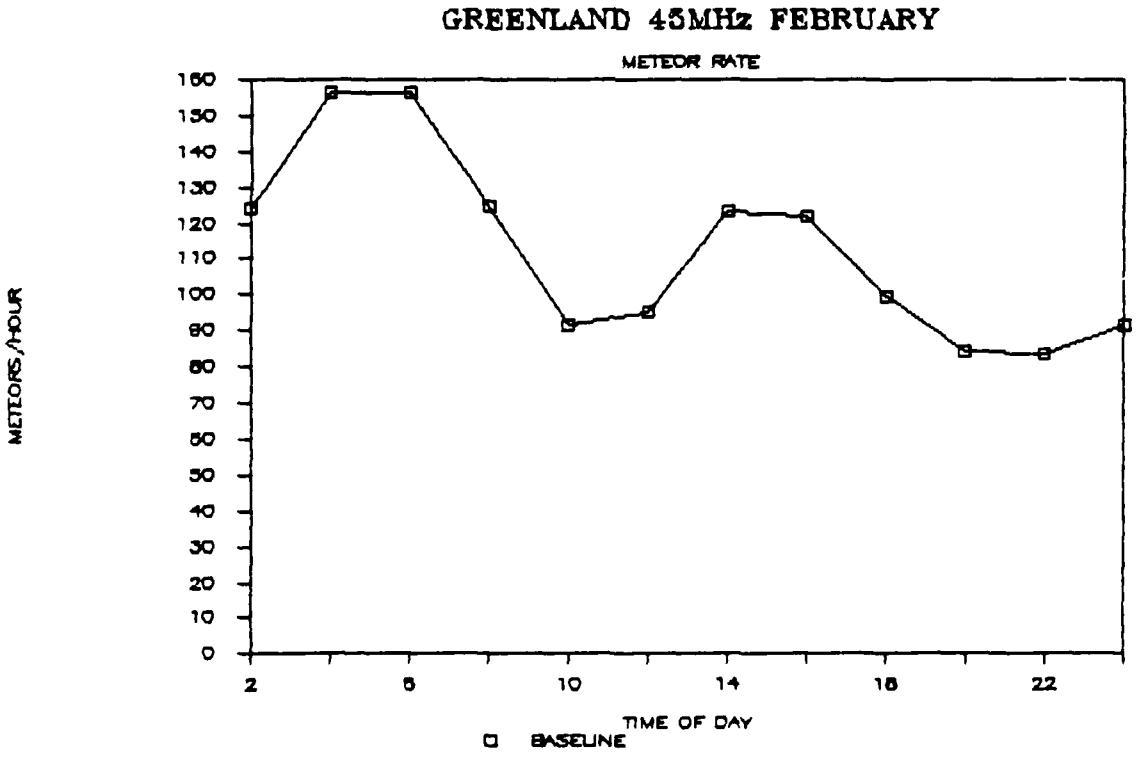

Figure 3-1. Baseline Greenland, February: Duty Cycle, Meteor Rate, Burst Length, Cosmic Noise

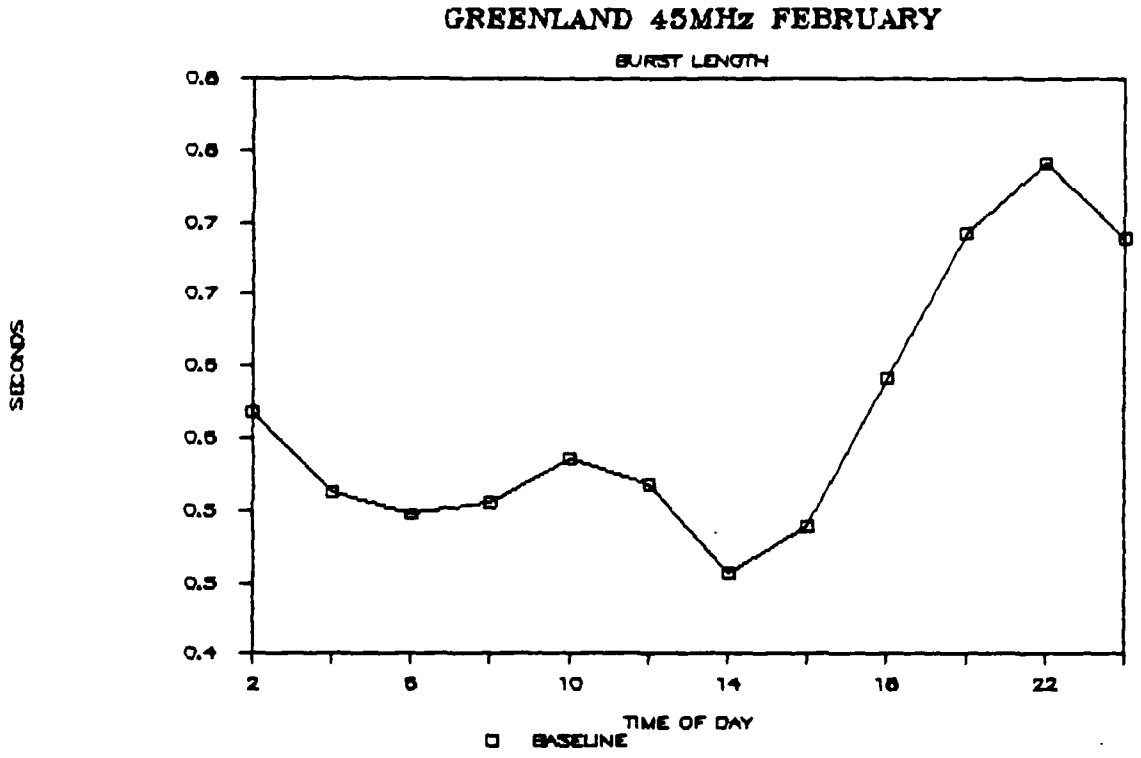

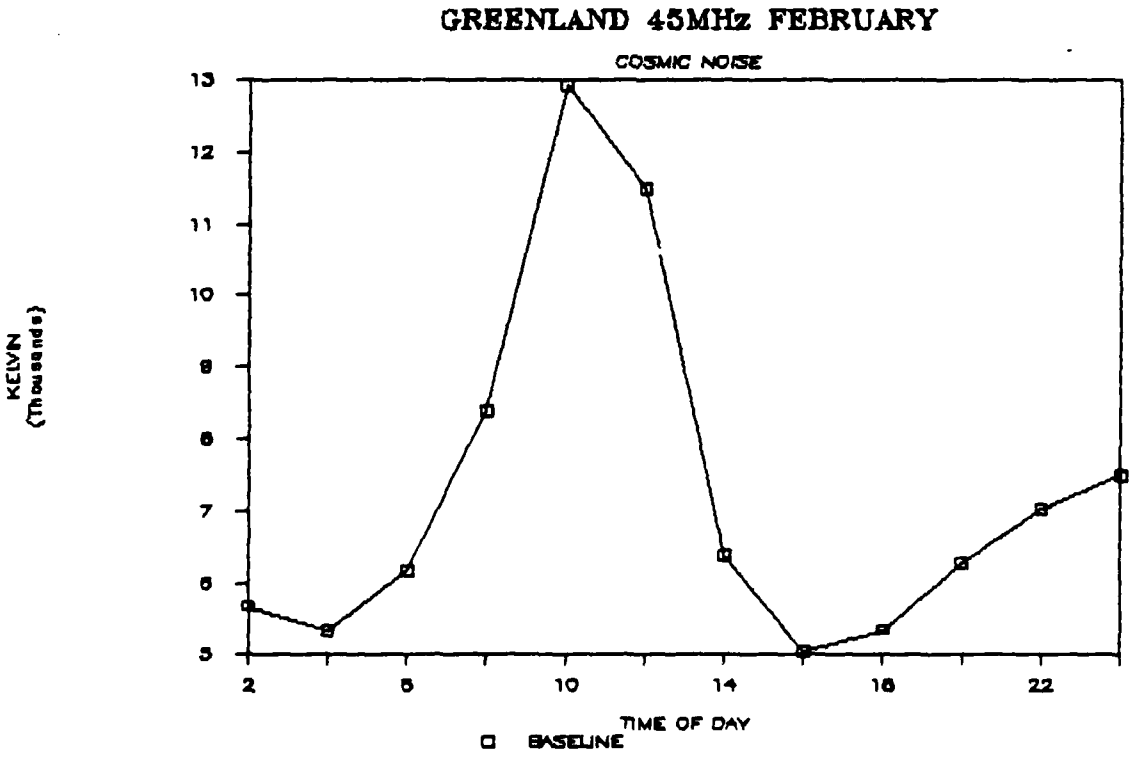

Figure 3-1. Baseline Greenland, February:
Duty Cycle, Meteor Rate, Burst Length, Cosmic Noise (Cont'd)

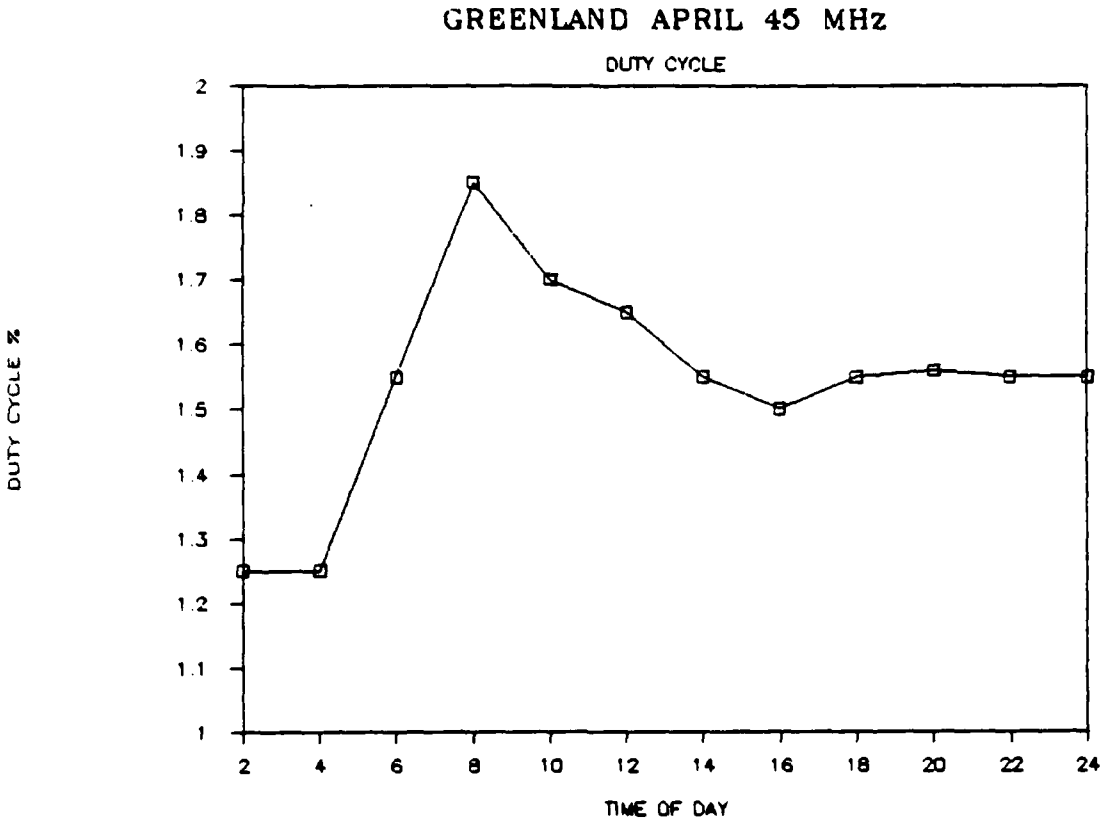

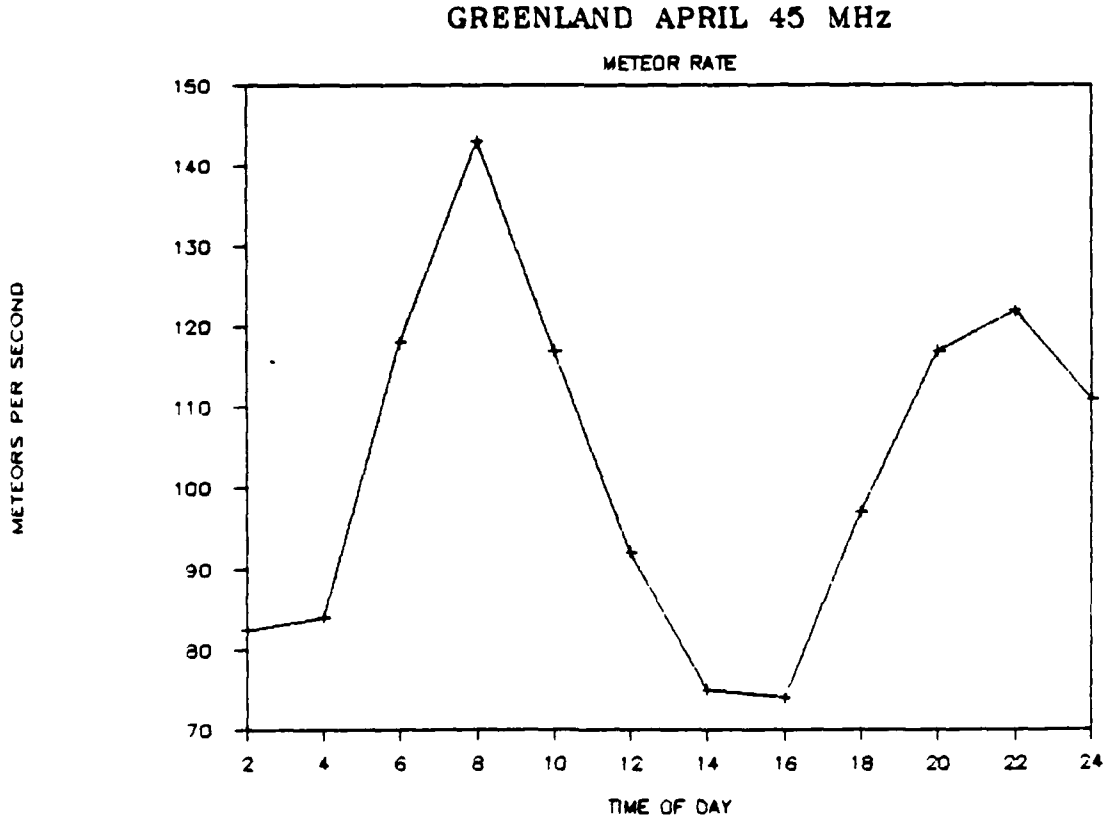

Figure 3-2. Baseline Greenland, April: Duty Cycle, Meteor Rate, Burst Length

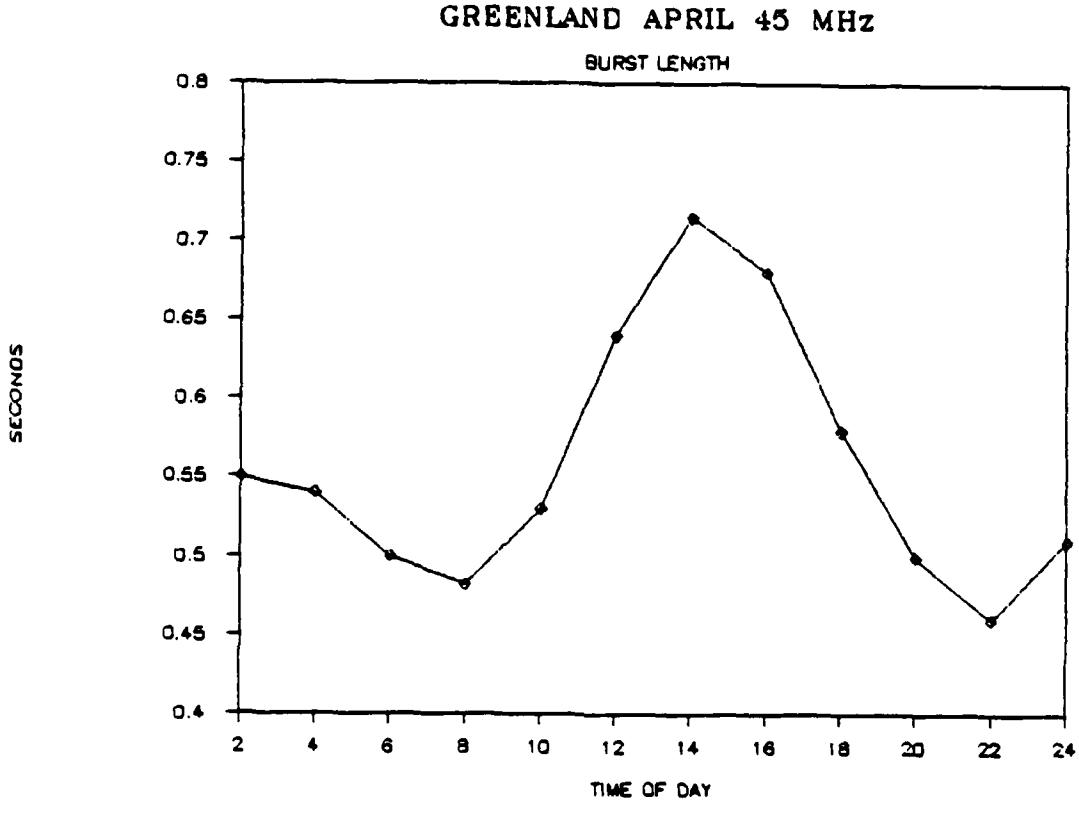

Figure 3-2. Baseline Greenland, April: Duty Cycle, Meteor Rate, Burst Length (Cont'd)

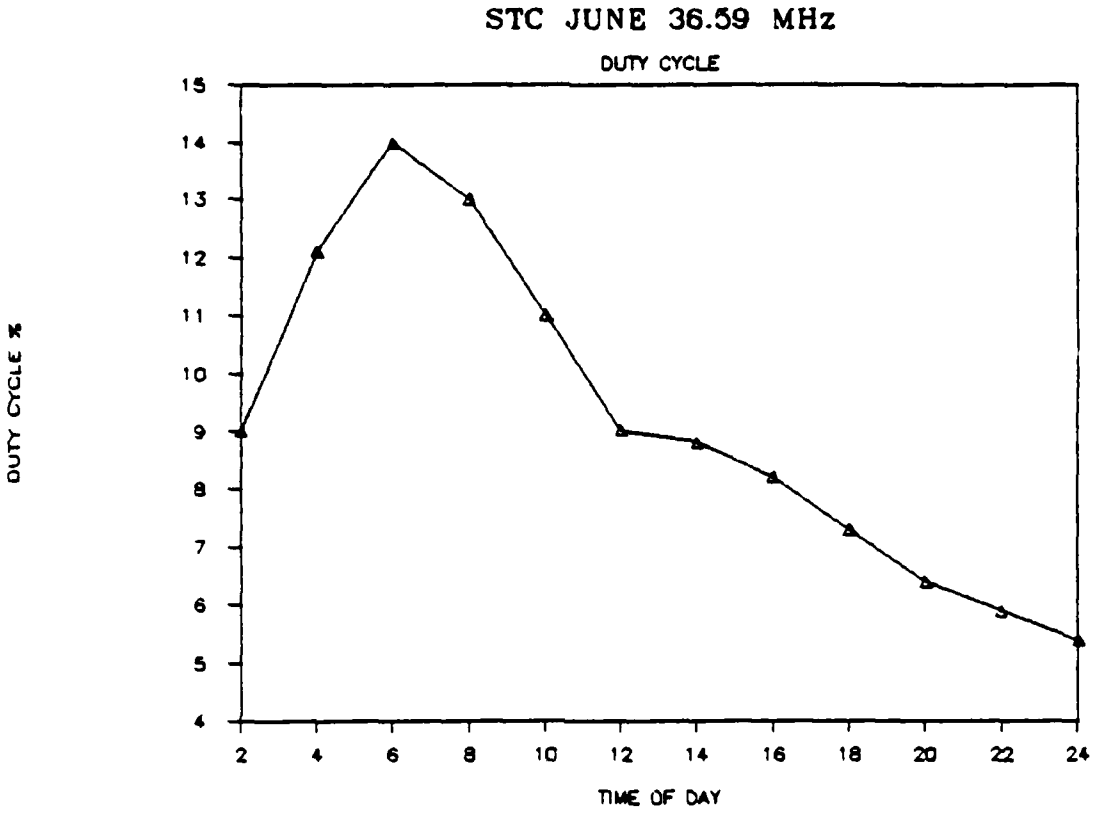

Figure 3-3. Baseline STC, June: Duty Cycle

SECTION 4 - ENHANCEMENT RESULTS

This section contains a description of each specific enhancement and presents test results showing its effect on the model. As in Section 3, plots of the enhanced model outputs are given for duty cycle, meteor rate, average burst length, and cosmic noise as appropriate to the particular enhancement. A superimposed copy of the baseline output is provided for ease of comparison in some cases.

4.1 IONOSPHERIC ABSORPTION EFFECTS

Polar Cap Absorption (PCA) results from increases in the low-energy cosmic ray flux from major solar flares. Energetic protons bombarding the ionosphere incite the absorption. The phenomenon appears several hours after a large solar flare and usually persists for a period of 1 to 6 days. The intensity of the effect varies with latitude and can last up to 10 days in the most northerly regions. During the event, strong HF/VHF absorption sets in over the polar cap, defined as the area north of about 64 degrees geomagnetic latitude. The absorption reaches its maximum within a few hours after the flare occurs and then slowly begins to decay. The intensity of the absorption is much higher during daylight hours, in contrast to auroral absorption, which is predominantly a nighttime event.

PCA has been modeled as an absorptive layer at altitudes extending from 60 to 80 km above sea level. The input is the vertical 30 MHz riometer reading in dB at path midpoint. The model calculates the absorption of individual uplink and downlink slant paths through the absorptive layer using the following equation:

$$a = a_o \left(\frac{30}{F}\right)^2 \csc(b)$$

where:

a	=	up-path or down-path attenuation in dB
a_o	=	riometer attenuation in dB
F	=	frequency in MHz
b	=	angle of incidence of the signal at the layer relative to the local vertical.

Plots of the baseline outputs from Section 3 are graphed in Figure 4-1 against results for PCA riometer readings of 0.5 dB, 1 dB and 5 dB. Graphs of the duty cycle, meteor rate, average burst length and cosmic noise are included for February for the Greenland link. As expected, the duty cycle, meteor rate and noise level drop as absorption increases. The noise decreases because the PCA layer absorbs cosmic noise as well as signal power. The average burst length increases with absorption since high power bursts tend to be long-lasting bursts.

4.2 HORIZON BLOCKAGE THAT VARIES WITH AZIMUTH

Obstruction of the horizon by hills or mountains can reduce performance on a meteor burst link. Horizon blockage is especially important on long meteor burst circuits where low takeoff angles are needed. The hot spots of meteor activity can be partially obstructed, thus reducing the number of meteor trails available.

The horizon blockage enhancement uses an array of azimuth angles and corresponding obstruction heights (in meters) and distances to the obstacle (in km). Azimuth angles to obstructions are referenced to true North and are positive to the East. Obstruction heights can be entered for any partial range of azimuth angles to model a quickly changing or a more gradually changing terrain. The terrain data should be entered feature by feature so that improper interpolations between near and far obstructions do not occur.

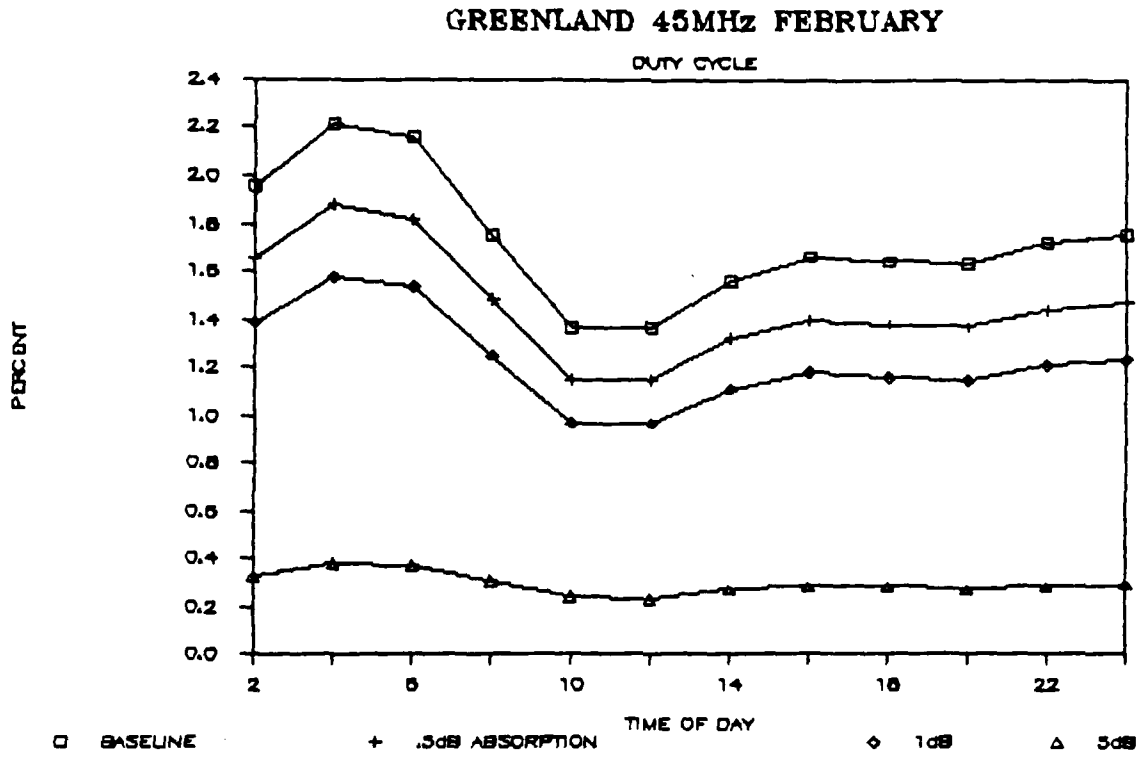

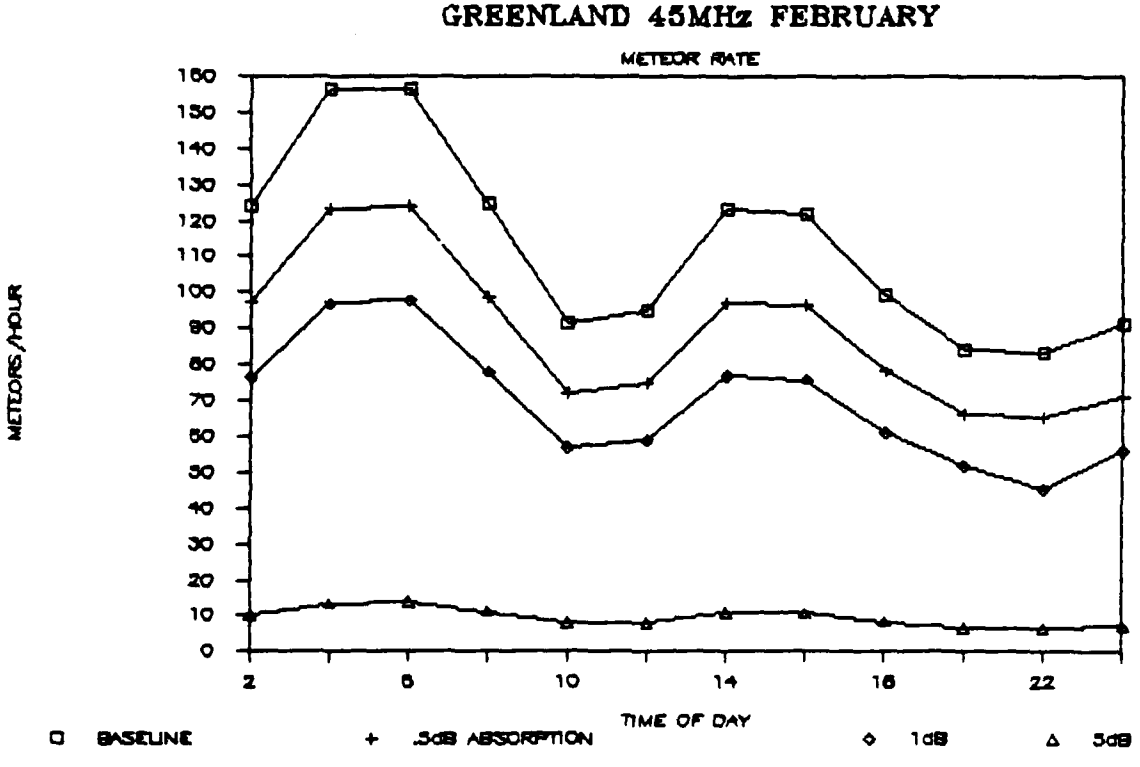

Figure 4-1. The Effect of Ionospheric Absorption on the Model Results

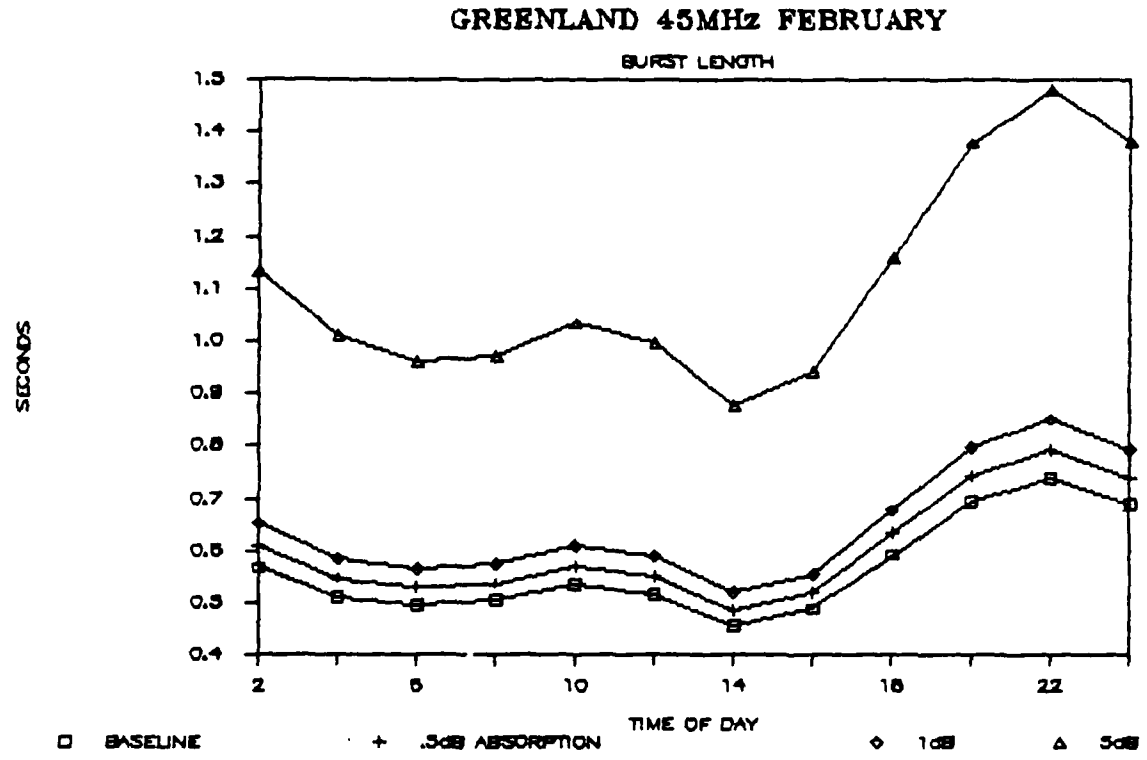

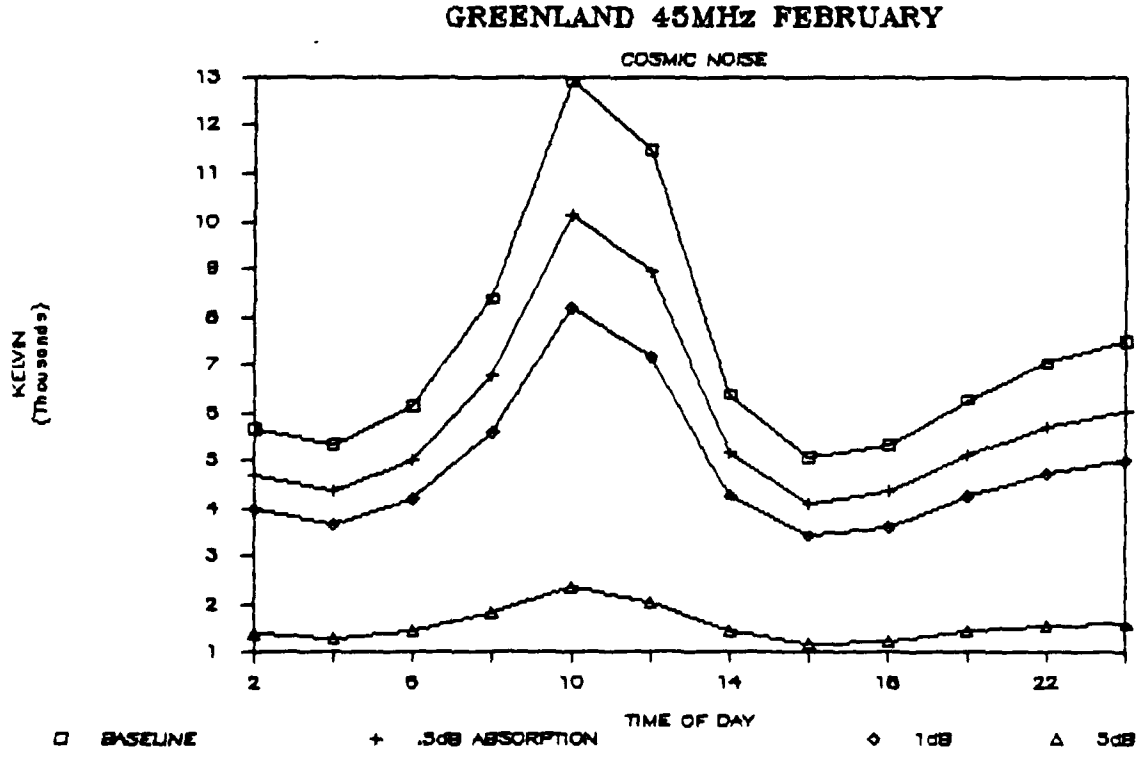

Figure 4-1. The Effect of Ionospheric Absorption on the Model Results (Cont'd)

To demonstrate the capability of the horizon blockage enhancement, results for a variety of conditions are presented below for the Greenland link:

- Test 1: Compare the case of blocking half the horizon at the transmitter only to the case of blocking the corresponding half of the horizon at the receiver only.
- Test 2: Compare the case of blocking the other half of the horizon at the transmitter only, to the case of blocking the corresponding other half of the horizon at the receiver only.
- Test 3: Block half of the horizon at the transmitter and block the opposite half of the horizon at the receiver.
- Test 4: Since the hot spots of meteor activity are largely to each side of the great circle path, compare for a fixed obstacle height and distance with results for varying widths of obstacle centered on the great circle path.

The results of Tests 1 and 2 for a high meteor activity time (06:00) are:

	BLOCK TRANSMITTER		BLOCK RECEIVER	
	DUTY CYCLE	METEOR RATE	DUTY CYCLE	METEOR RATE
Test 1	1.49%	97.29/hr	1.49%	97.29/hr
Test 2	.67%	59.13/hr	.67%	59.13/hr
No Blockage	2.16%	156.42/hr		

Test 1 results are as anticipated, the results are identical for blocking out the corresponding side of the sky at each site separately. Test 2 results show that the values are also identical for blocking out the other half of the sky at each site separately. An additional check shows that the sum of the results from blocking each of the two halves is equal to the whole - the case of no blockage.

The results of Test 3 demonstrated that indeed blocking opposite halves at the same time does obstruct the entire sky, reducing duty cycles and meteor rates to zero.

For Test 4, an obstruction 1,000 km high and 10 km from the transmitter was centered on the transmitter to receiver bearing angle. As shown in Figure 4-2, for blocking angles less than 5 degrees, no significant loss of duty cycle was found since the meteor activity hot spots to the side of the great circle path are not significantly obscured. The duty cycle is reduced by a half at 12 degrees for both high and low meteor activity times.

4.3 AIRBORNE TERMINAL CAPABILITY

The CSC meteor burst model as originally implemented assumed that the transmitter and receiver were on the ground; the modeling of the spherical earth assumed that negative takeoff angles were impossible. The removal of this shortcut required sweeping changes throughout the model. The model now handles cases of elevated transmitter and/or receiver terminals with values up to 30,000 meters above sea level for either site. The exact approach taken to the geometry of the elevated terminal case had an interesting side effect; it removed a several-hour error in the time of the cosmic noise maximum on the Greenland link.

This enhancement was tested using two meteor burst paths; the Greenland link discussed in Section 3 (1209 km path length) and a very long east-west link on the Equator (2000 km path length). The tests to follow show how duty cycle is influenced by an elevated terminal.

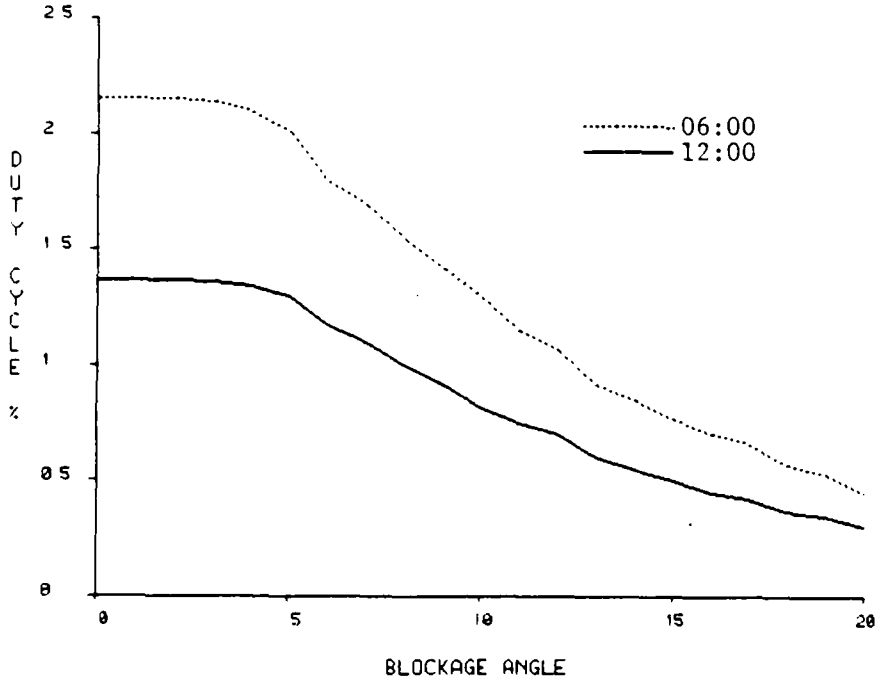

Figure 4-2. The Effect of Obstructing the Horizon at the Transmitter on the Greenland Link

The model uses six heights from a lowest of 81 km to a highest of 111 km as the basis of the duty cycle calculations. The farthest distance at which a terminal can see a potential meteor trail at the 111 km height is given by the sum of D_1 and D_2 where:

$$D_1 = R \left(\text{ASIN} \left(\frac{R}{R+H} \right) - \frac{\pi}{2} \right)$$

where

H = terminal height in km

R = radius of the earth = 6370 km

and

$$D_2 = R \left(\text{ASIN} \left(\frac{R}{R + 111 \text{ km}} \right) - \frac{\pi}{2} \right)$$

Figure 4-3 shows how the sum of D_1 and D_2, the visibility limit, varies with the height of a terminal above the ground.

Basically, one would expect that as terminals are elevated, performance would improve because the common volume of the transmit and receive antennas increases. The duty cycle of a long link will start near zero for terminals on the ground and increase as terminal elevations increase. This is graphically shown in the 3-D plots of the duty cycle results from the enhanced model for transmitter heights of 0 km, 7.5 km and 25 km in Figure 4-4. The circles represent the transmitter and receiver sites and the arrow points north; the circle on the right is the elevated transmitter. Values are calculated at the intersections of the grid lines, which are spaced for a Gaussian integration. The values plotted are the sum of values for that point at the six heights in the ionosphere spanning the regions of meteor ionization. The graph at 0 km has been scaled up by a factor of 10 compared to the other heights.

The Greenland link's duty cycle increases a small amount at first as the terminal is elevated. The duty cycle then levels off and shows no perceptible gain as the terminal is raised further.

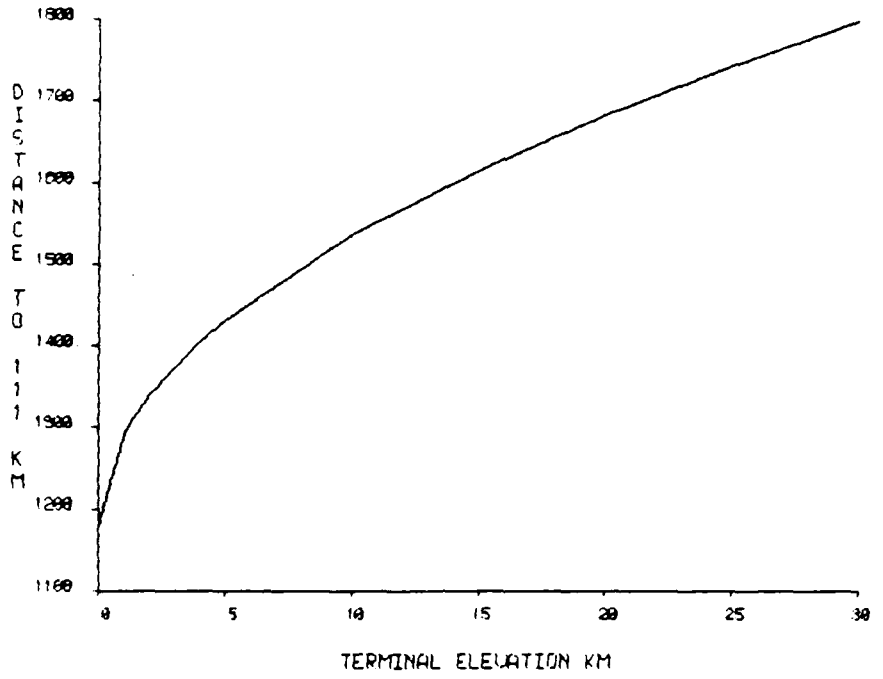

Figure 4-3. Maximum Range at Which a Potential Meteor Trail at 110 km Altitude Can Be Observed

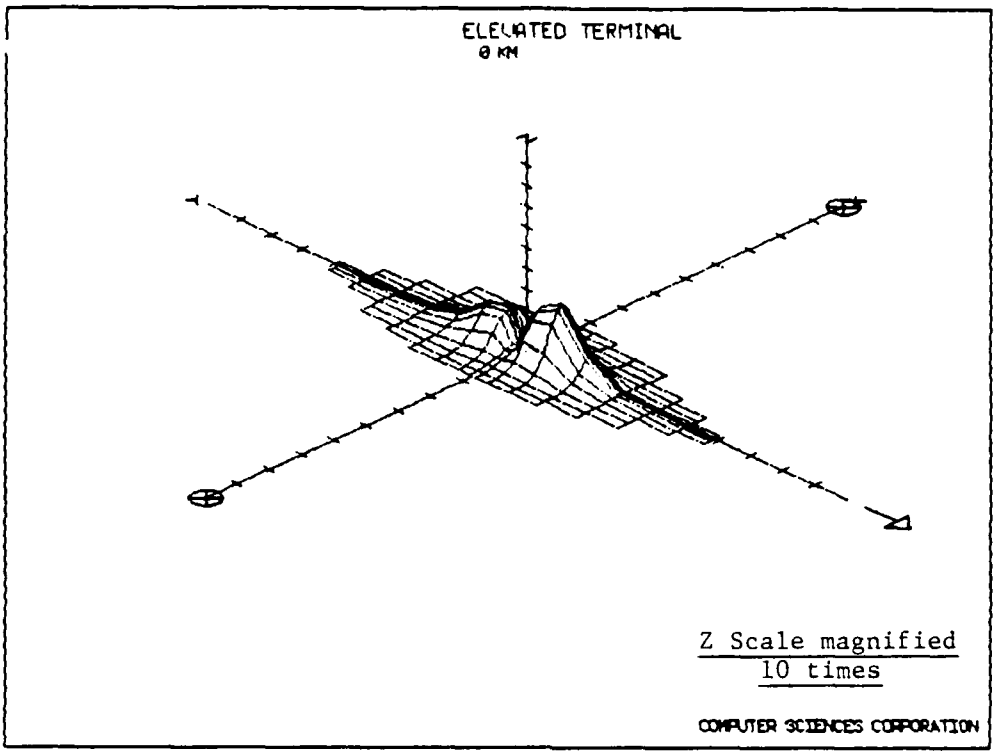

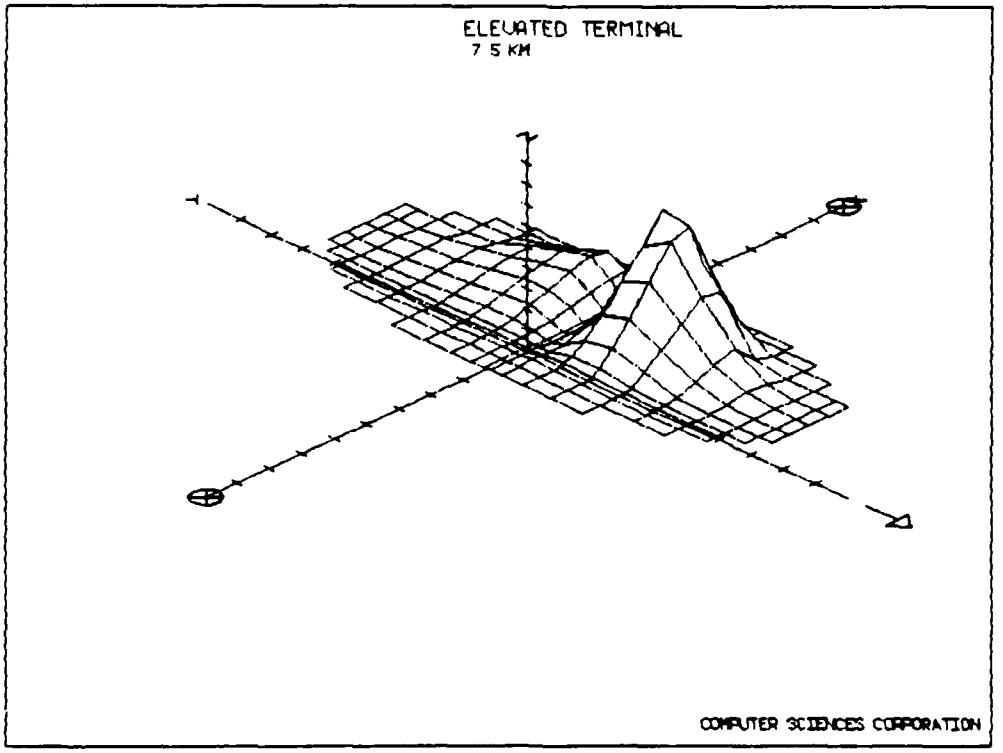

Figure 4-4. Hot Spot Sizes and Horizon Location for a Long Path and One Terminal Elevated to 0, 7.5 and 25 km

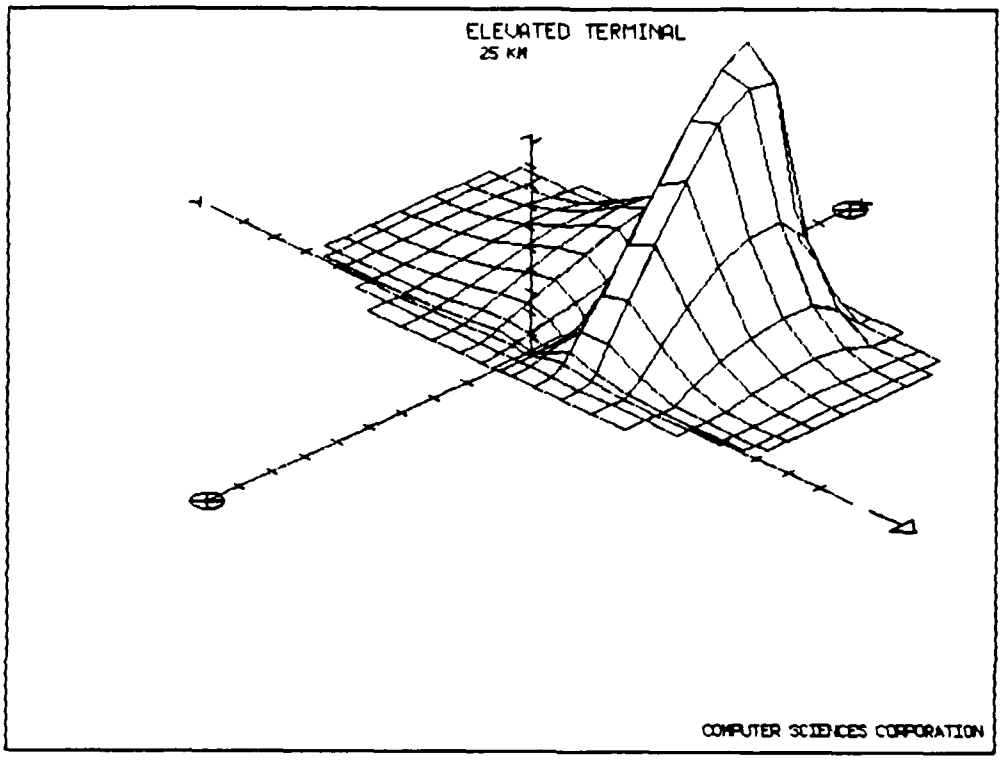

Figure 4-4. Hot Spot Sizes and Horizon Location for a Long Path and One Terminal Elevated to 0, 7.5 and 25 km (Cont'd)

This is due to the fact that for this medium length link, the hot spots are almost completely covered by antennas on the ground and increasing elevation doesn't contribute significantly to duty cycle. This is graphically shown in Figure 4-5. The hot spots are essentially the same for all heights up to the 30,000 meter limit. The duty cycle results of the elevated terminal tests are shown in Figure 4-6. The model appears to handle elevated terminals in a manner which is qualitatively correct.

4.4 EARTH'S GRAVITATIONAL EFFECT

A meteor's geocentric velocity, V, at the earth's distance from the sun is approximately the vector sum of the meteor's heliocentric velocity, V_H, and the earth's orbital velocity V_e. Newton's law of gravitation states that any two masses attract each other with a force directly proportional to their masses, and inversely proportional to the square of the distance separating their centers of mass. A meteor starting at rest at an infinite distance from the earth will attain a velocity given by $V_f^2 = 2GM_e/r = 125\ km^2/sec^2$, where the gravitational constant $G = 6.67 \times 10^{-19}$ Newton km^2/kg^2, and the earth has a mass $M_e = 5.98 \times 10^{24}$ kg with a radius $r = 6.37 \times 10^3$km.

Corrections due to the rotation of the Earth on its axis and the viscous nature of the atmosphere are small relative to V and the effect of gravity. The geocentric velocity V_g, taking the Earth's gravity into account, can then be written as:

$$V_g^{\ 2} = 125 + V^2 \quad km^2/sec^2$$

where V_g is the geocentric velocity of the meteor and V is the geocentric velocity of the meteor before coming under the influence of the Earth's gravity.

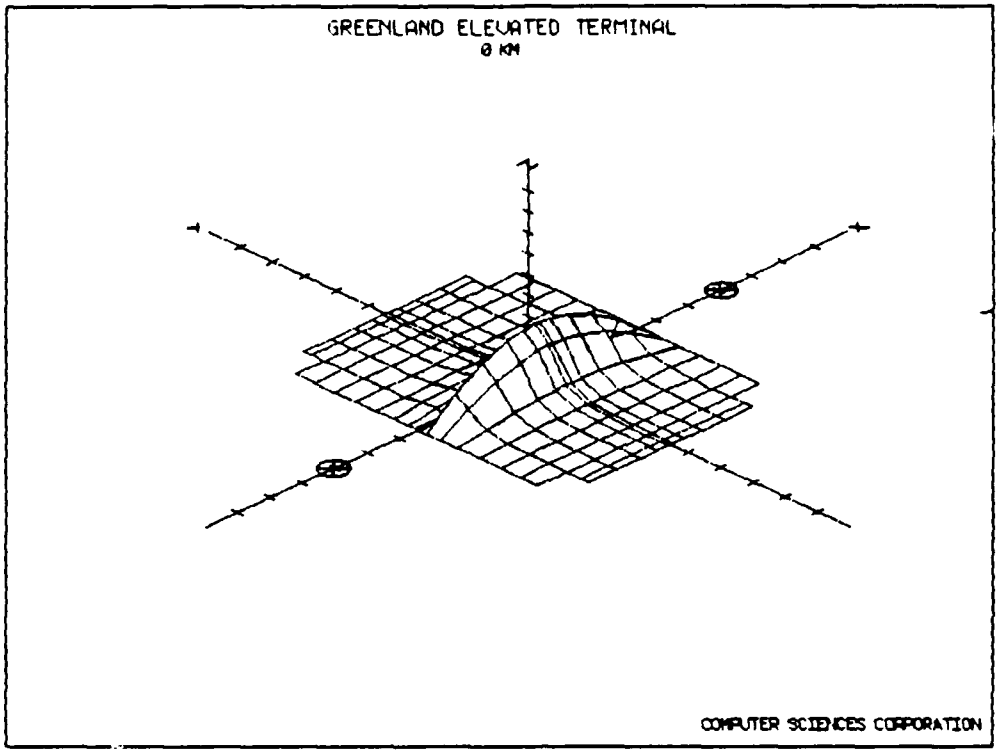

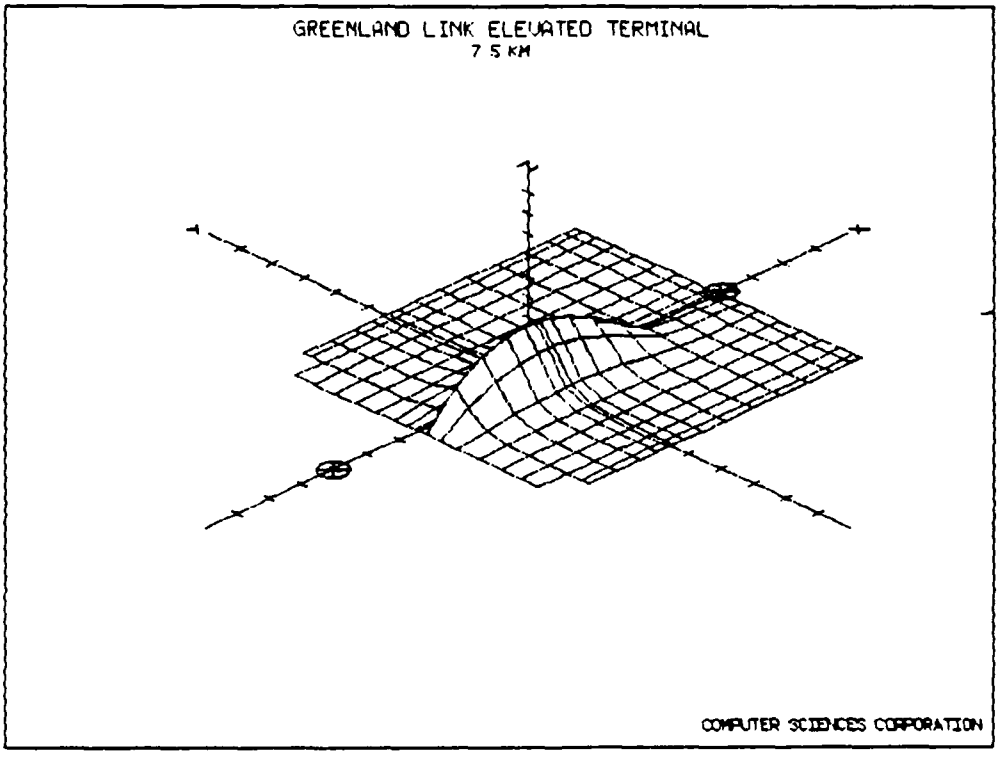

Figure 4-5. Hot Spot Sizes and Locations for the Greenland Link as One Terminal is Elevated to 0, 7.5 and 15 km

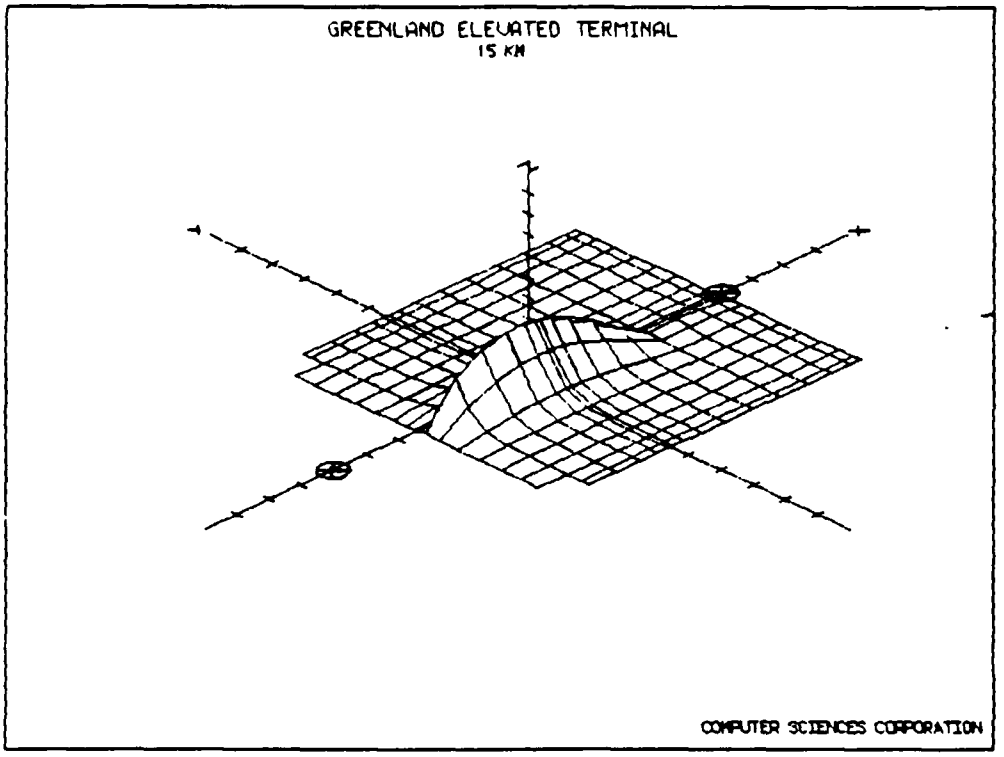

Figure 4-5. Hot Spot Sizes and Locations for the Greenland Link as One Terminal is Elevated to 0, 7.5 and 15 km (Cont'd)

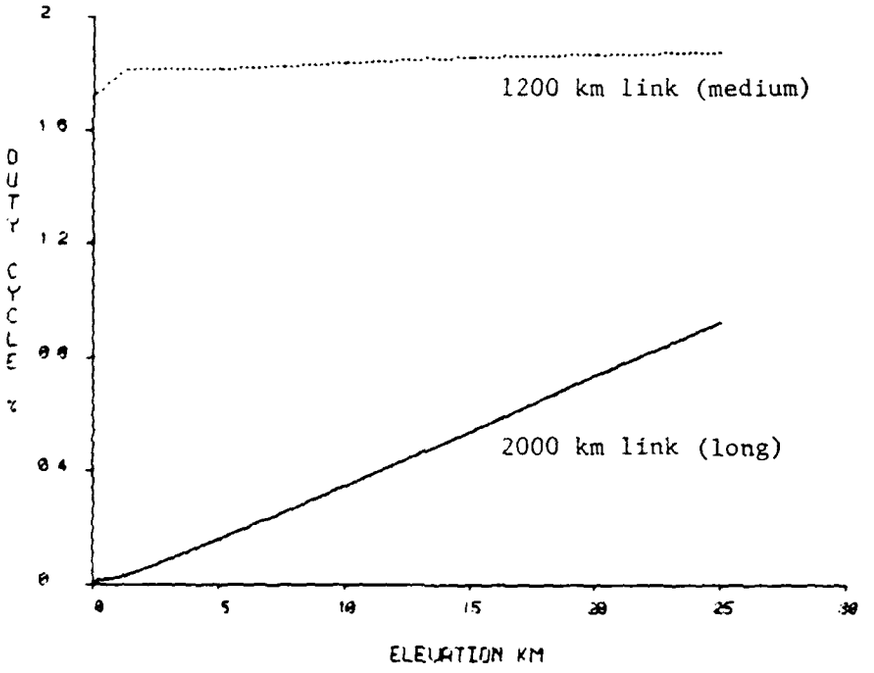

Figure 4-6. Duty Cycle Versus the Elevation of One Terminal of a Medium Length and a Long Meteor Burst Circuit

The CSC meteor burst model uses a varying velocity V_g based on observational data and geometry. Sporadic meteors move in mutually unrelated orbits and the Earth's motion through them will cause both the meteor rate and the average meteor velocity to be the highest on the "front" side of the Earth, the "apex" of the Earth's way. The diurnal variation of the average meteor velocity has been modeled as:

$$V_g = 40.0 + 5.0 \cos \theta$$

where θ is the angle between the Earth's apex vector and the zenith vector at the midpoint of the meteor burst path. Figure 4-7 shows the diurnal variation resulting from this equation for a mid-northern latitude in June. Note the asymmetry about 40 degrees and the fact that the full ± 5 degrees swing is not realized.

Figure 4-8 shows the sensitivity of the model results to the average meteor velocity. This sensitivity is due to the relationship between ionization production and meteor velocity. Figure 4-9 shows a comparison of model results using a velocity variation based on the above equation and the baseline, which used a velocity of 40 km/sec in all cases. The result is in accord with expectations: high velocity meteors burn up higher in the ionosphere and therefore have shorter durations than lower velocity meteors.

Gravity affects not only the meteor's velocity but also its trajectory. The paths of meteors approaching Earth are altered as they come under the influence of the Earth's gravitational field. Zenith attraction is this change of the meteor's radiant as observed from earth with respect to its true radiant.

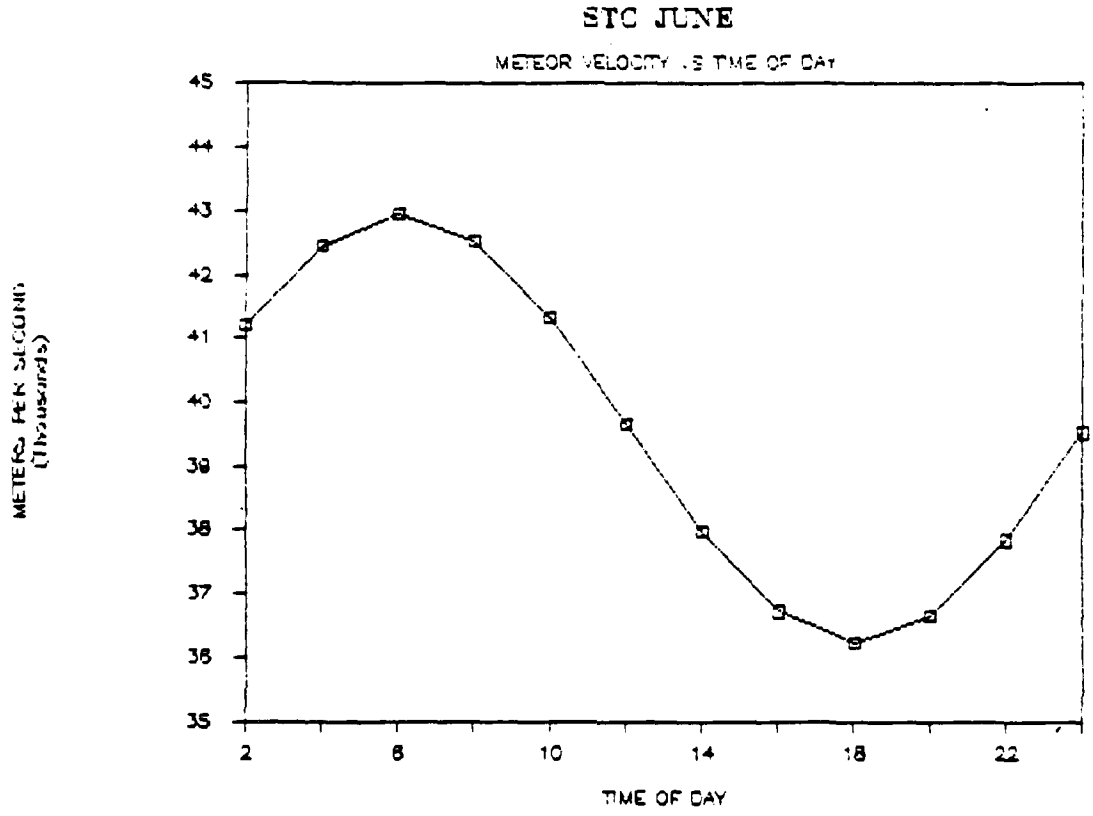

Figure 4-7. The Diurnal Variation in Average Meteor Velocity Calculated by the Model for the STC Link in June

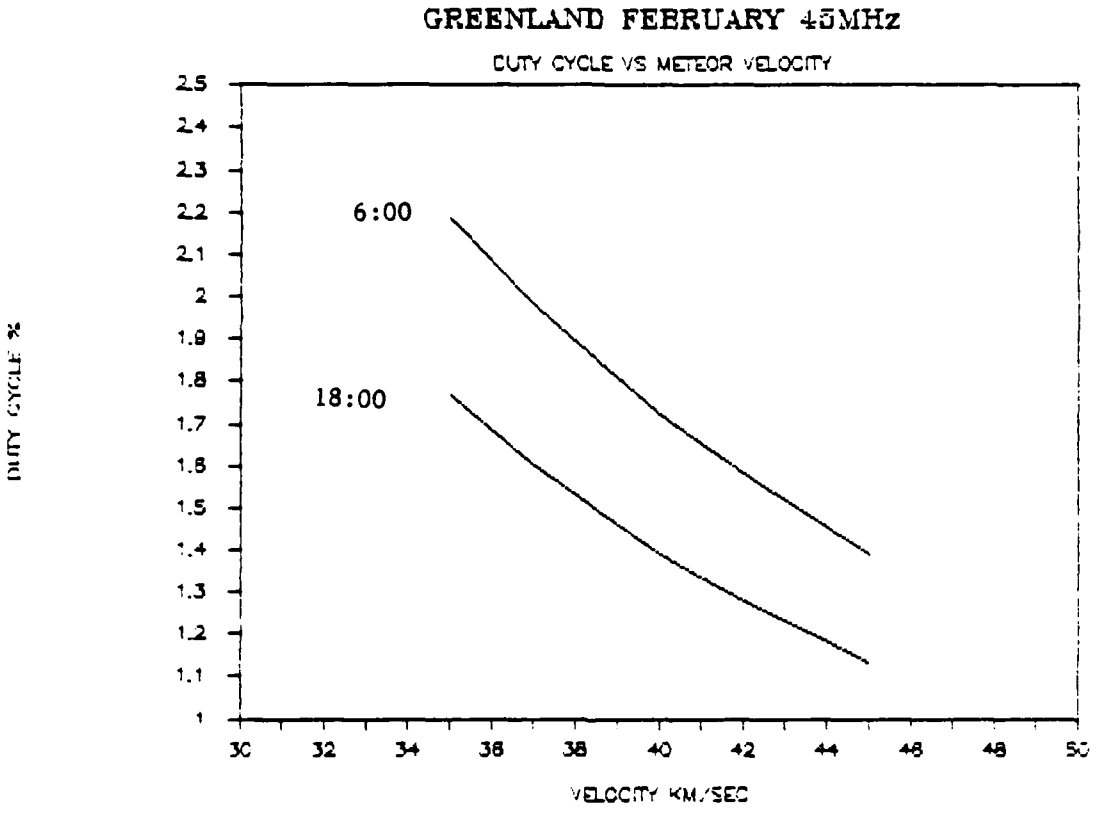

Figure 4-8. The Effect of Average Meteor Velocity on Duty Cycle with All Other Parameters Kept Constant

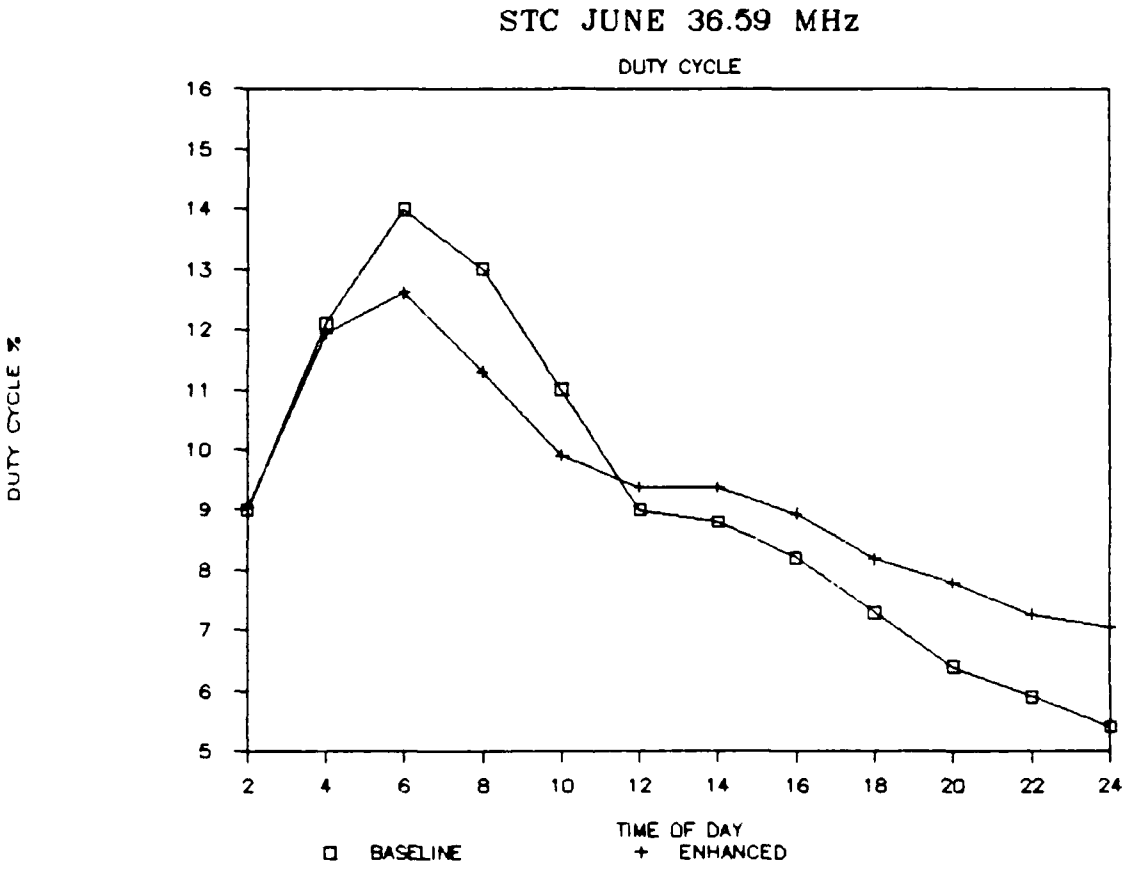

Figure 4-9. The Effect of the Average Velocity Model on Duty Cycle

The CSC model uses the following equation to obtain a meteor's change in direction ΔZ, with respect to the observer's zenith:

$$\tan\left(\frac{\Delta Z}{2}\right) = \frac{V_g - V}{V_g + V} \tan\left(\frac{Z}{2}\right)$$

where Z is the zenith angle of the meteor trail. This equation is used to correct an observed radiant to a true radiant for which the meteor flux is known. The effect is very small as shown in Figure 4-10 which shows the effect of zenith attraction on the STC link duty cycle baseline and on the combined zenith attraction and velocity variations.

4.5 OVERDENSE BURST AND TRANSIENT/RESONANCE EFFECTS

At low electron densities, the underdense case, an incident wave passes through the meteor ionization trail without major modifications. At high electron densities, the overdense case, the incident wave penetrates the trail only until reaching an area of sufficiently high electron density and the trail, then, essentially acts as a reflecting metallic column. After a time, the electron density in an overdense trail falls below the transition value and the underdense model is again applicable.

Overdense trails are modeled exactly as specified in Reference 1 and the transition from underdense to overdense is taken as a line density of 0.75×10^{14} electrons/meter since this value gives the same power from the underdense and overdense equations.

The model now covers the case where the burst duration is not long compared to the trail formation time. The maximum signal level will be slightly reduced since parts of the trail will decay before it is totally formed. Overdense meteors, on the other hand, produce relatively long duration signals. The transients of trail formation have much less effect on the peak amplitude and duration of overdense trails than on those of underdense trails.

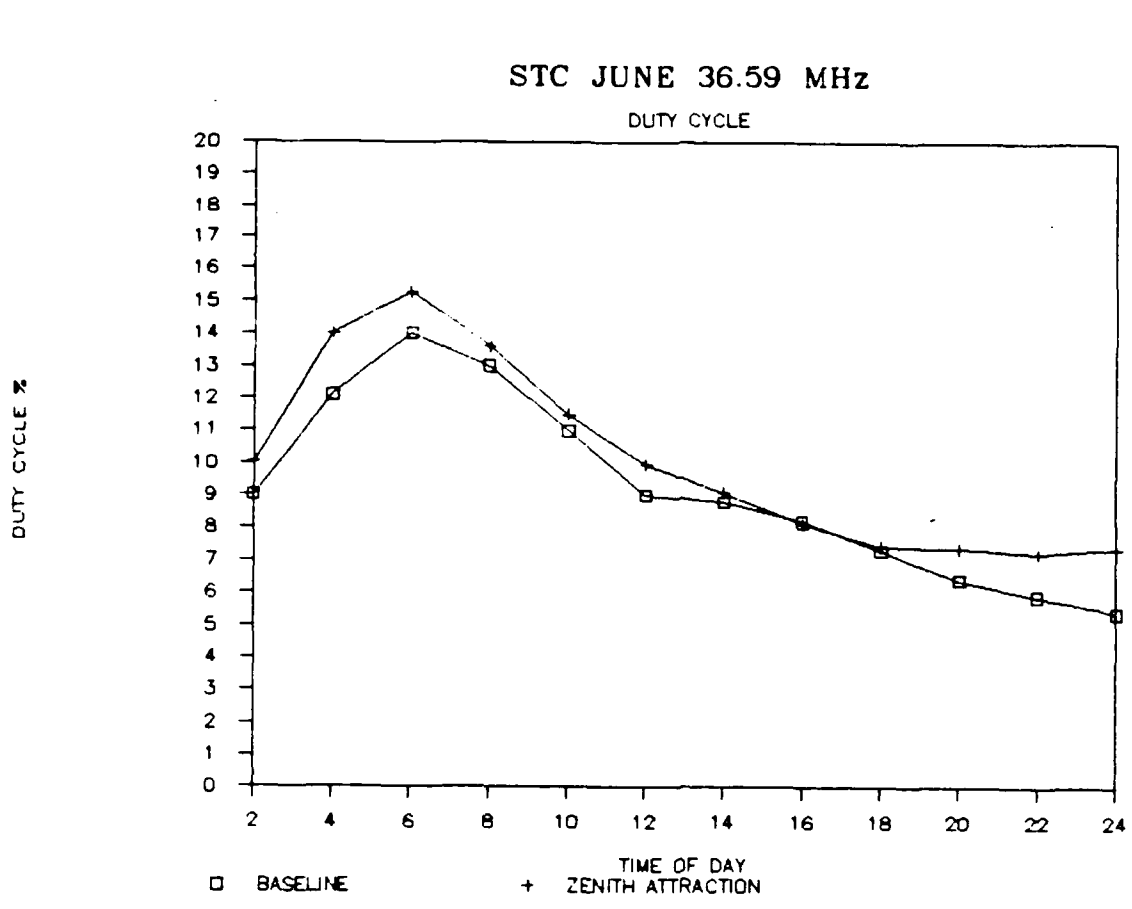

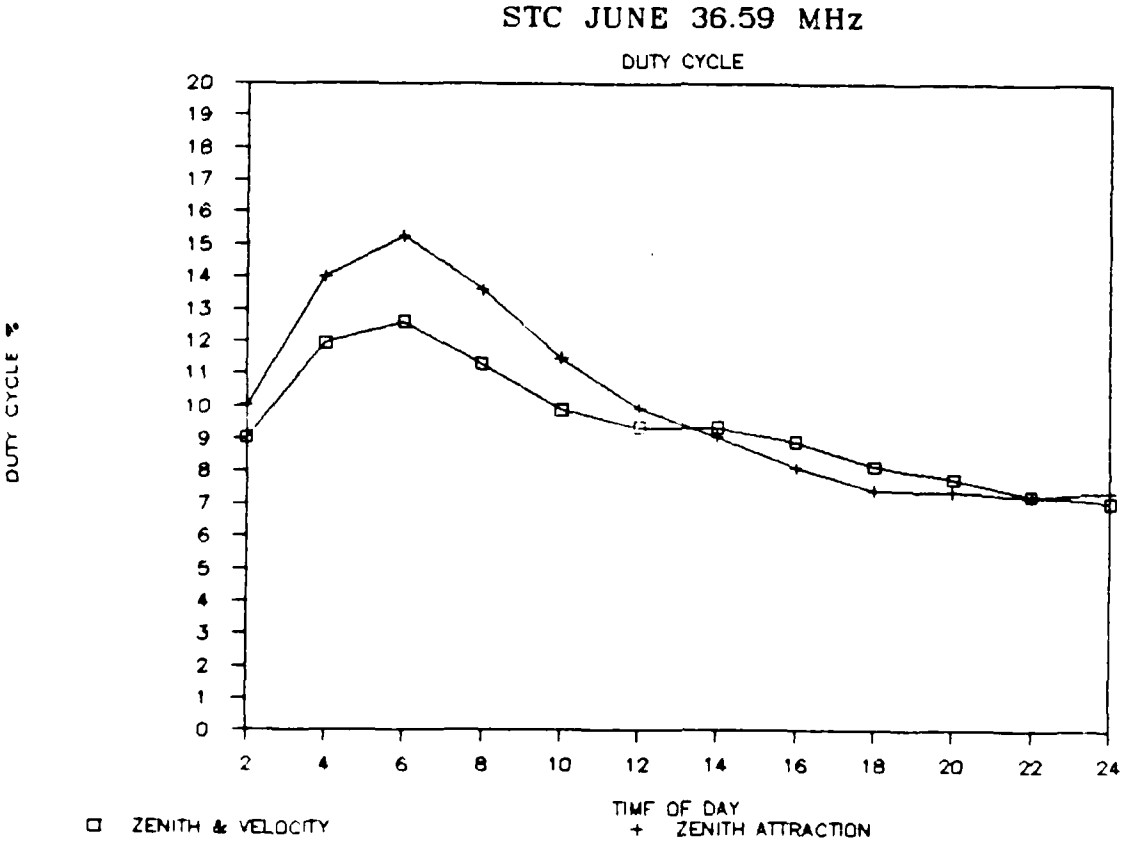

Figure 4-10. The Effects of Zenith Attraction and Velocity Variation on the STC Link

The overdense enhancement results are shown in Figure 4-11 for the Greenland link in April against the baseline results of the underdense model only. These results include the effects of overdense meteors, burst formation effects and meteor velocity variation. The overdense model is responsible for the large increase in burst duration. Such large durations are not, of course, correct; they greatly exceed what would be measured. However, the results are correct in the sense that the algorithms laid down in Reference 1 have been correctly implemented. Any physical computer model has as its basis a number of constants that may not be known very accurately. Burst duration is particularly sensitive to the values of atmospheric variables such as the diffusion constant, atmospheric pressure at the heights in question, and initial radius of the ionization trail. Initial tests suggest that the burst duration can be brought into agreement with measured results by relatively small changes of the expression used to calculate diffusion - changes well within the rather large uncertainty which seems to exist regarding the value of this parameter. The correct setting of this parameter will be determined in Subtask 2 of this effort which concerns Model Validation.

Previously the model tacitly assumed that the incident electric vector was parallel to the axis of the meteor trail. However, in the majority of cases, the incident electric vector will have a component transverse to the trail. This transverse field tends to displace electrons in the trail which are then influenced by a restoring force from the more massive positive ions in the meteor trail. This interplay of forces produces a resonance effect which can lead to an increase in the amplitude of the scattered signal.

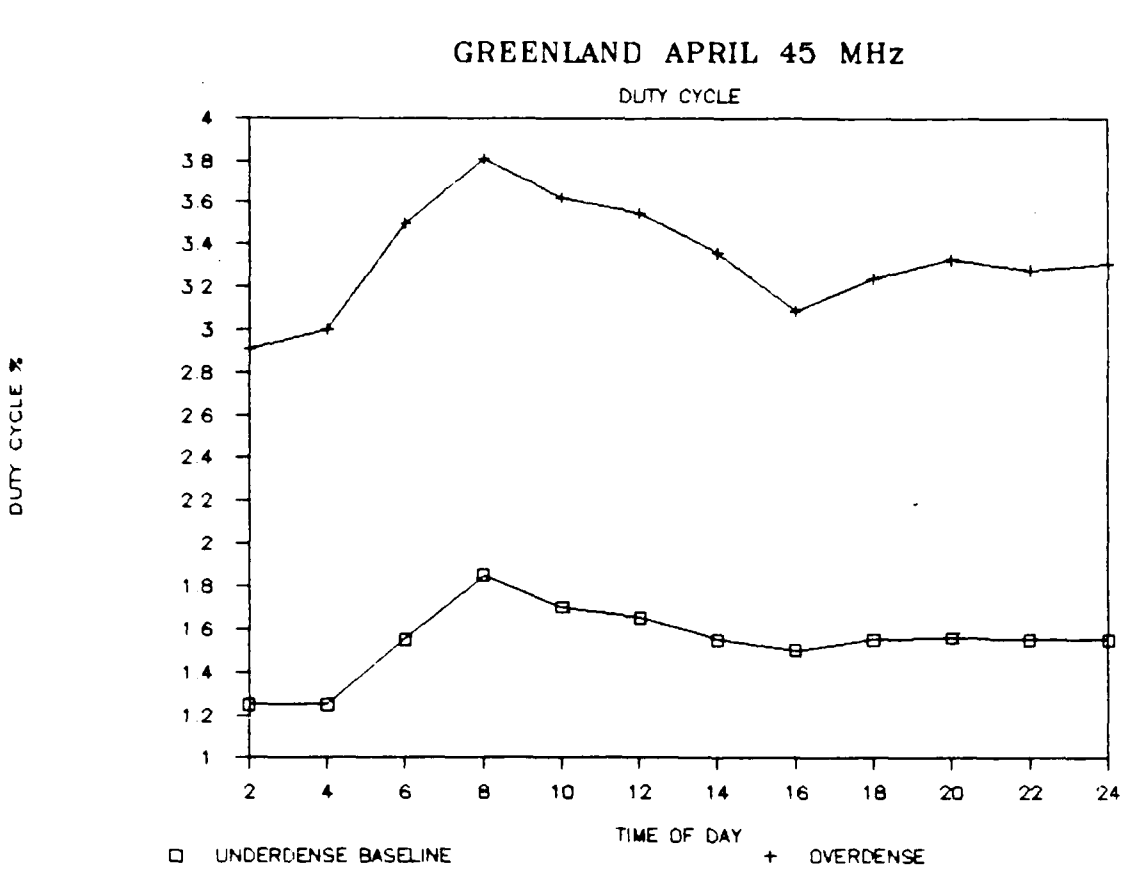

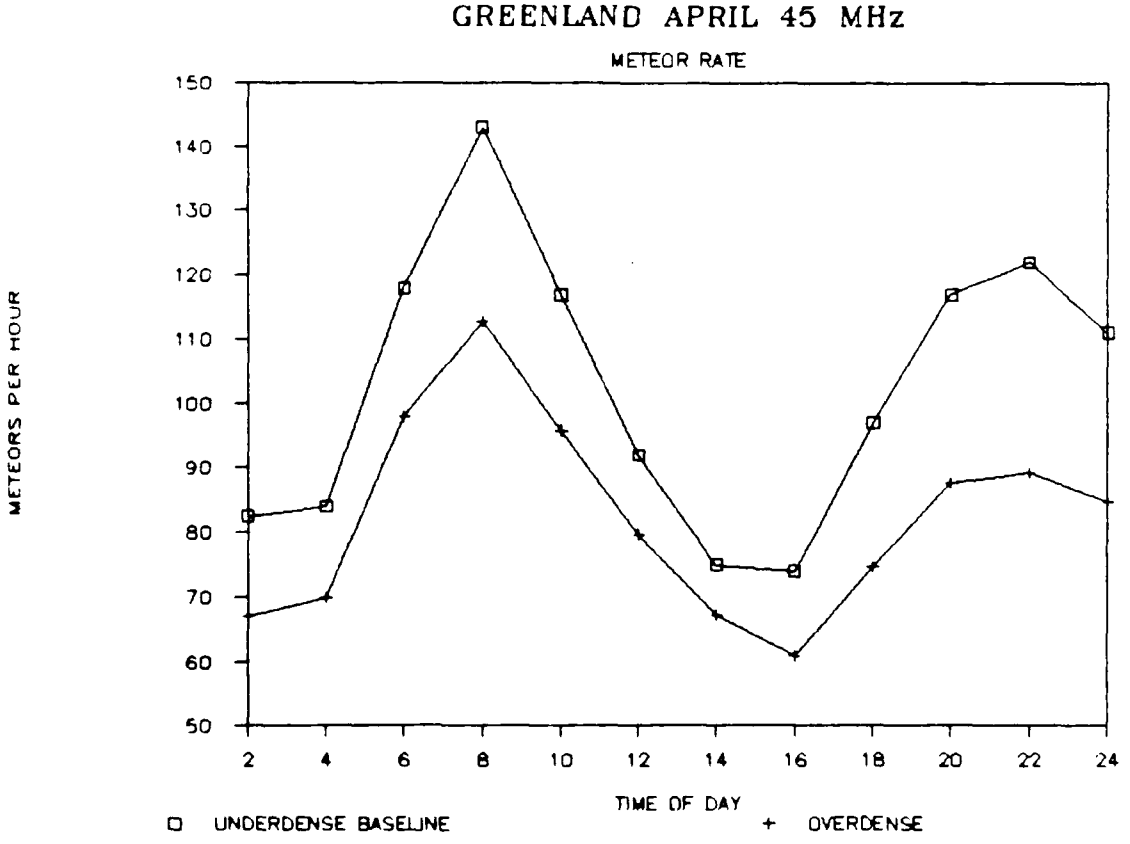

Figure 4-11. The Effect of Overdense Burst Modeling on the Greenland Link

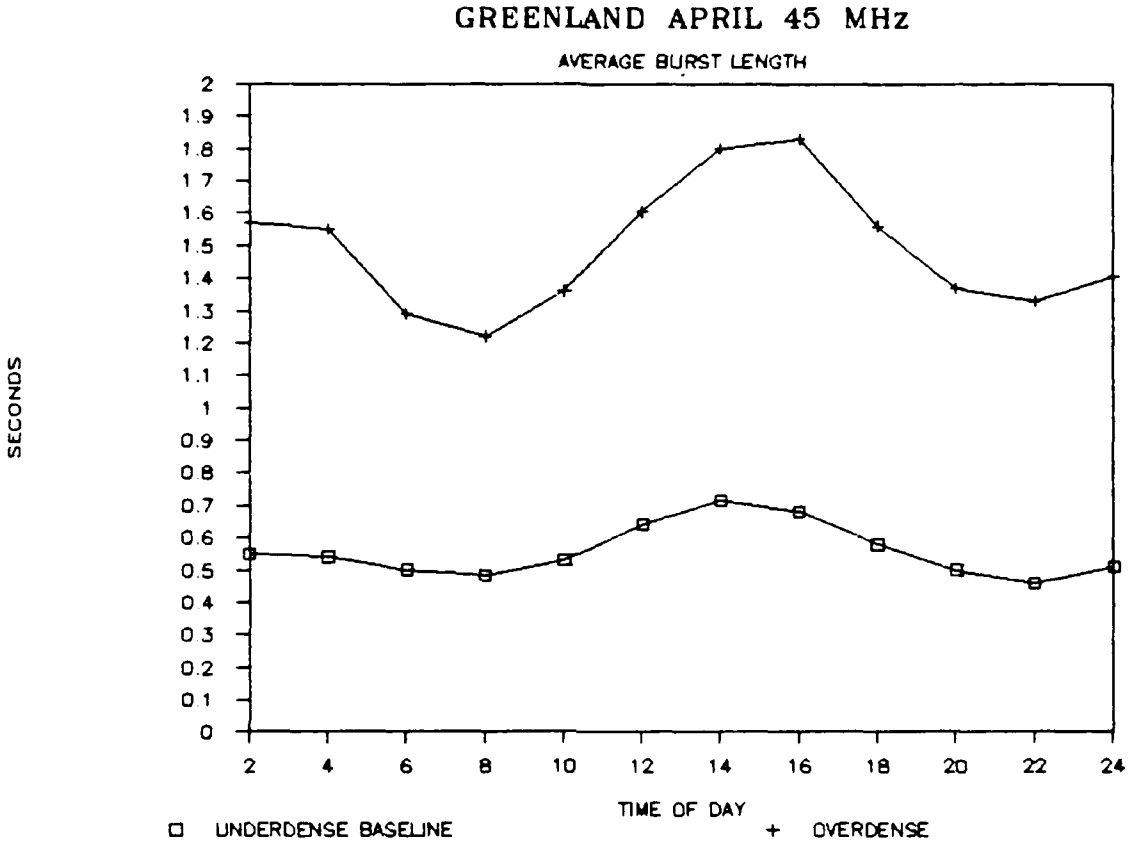

Figure 4-11. The Effect of Overdense Burst Modeling on the Greenland Link (Cont'd)

Figure 4-12 shows the results from the previous test concerning explicit overdense burst modeling compared to the case in which transverse resonance on underdense bursts is also modeled.

4.6 LOWER ATMOSPHERIC REFRACTION

Based on user inputs of the refractivity constant normalized to mean sea level and the terminal elevations, the enhanced model calculates a refractivity profile for the transmit and receive terminals. For meteor burst links where both terminals are elevated and for short to medium path lengths, lower atmospheric refraction effects will normally be negligible. For longer paths between terminals at sea level, refraction can be important because of the extra common volume for the potential meteor trails that may result.

This enhancement is modeled as specified in Reference 1. The model calculates the amount of ray bending on each propagation path. Lookup tables are generated for the transmitter and receiver sites to provide the total bending angle versus takeoff elevation angle.

The refraction enhancement test results are shown in Figure 4-13 for a long east-west link on the Equator (2000 km path length). These results include the effects of the refraction enhancement only and the hot-spot diagram should be compared to the 0 km terminal height in Figure 4-4 found in section 4.3 to see that indeed the performance improves as the common volume of the transmit and receive antennas increases.

Figure 4-14 shows the effect of refraction on a medium length path (Greenland link). This hot-spot diagram should be compared to the 0 km terminal height diagram found in Figure 4-5 in section 4.3. Only negligible gain is realized as predicted due to the fact that the hot spots are almost completely covered by the antennas in the absence of refraction. The refraction enhancement is, therefore, qualitatively correct.

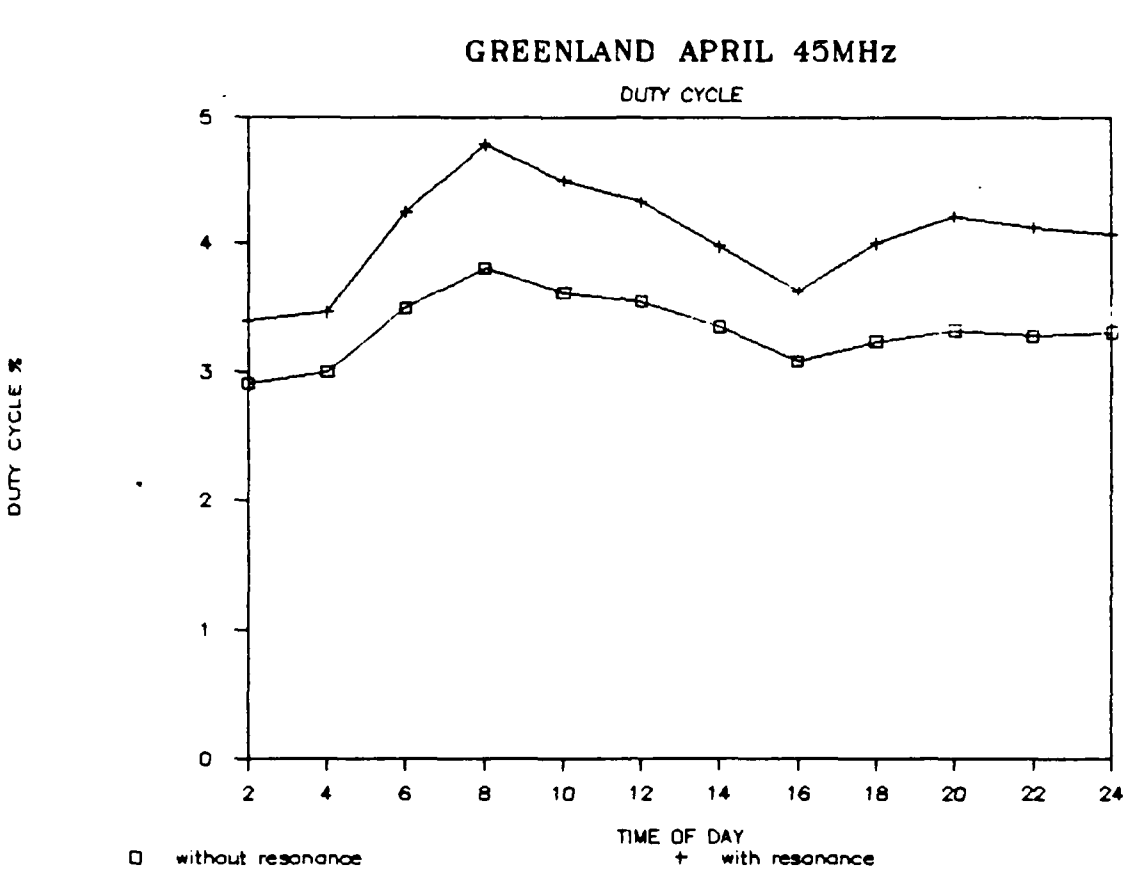

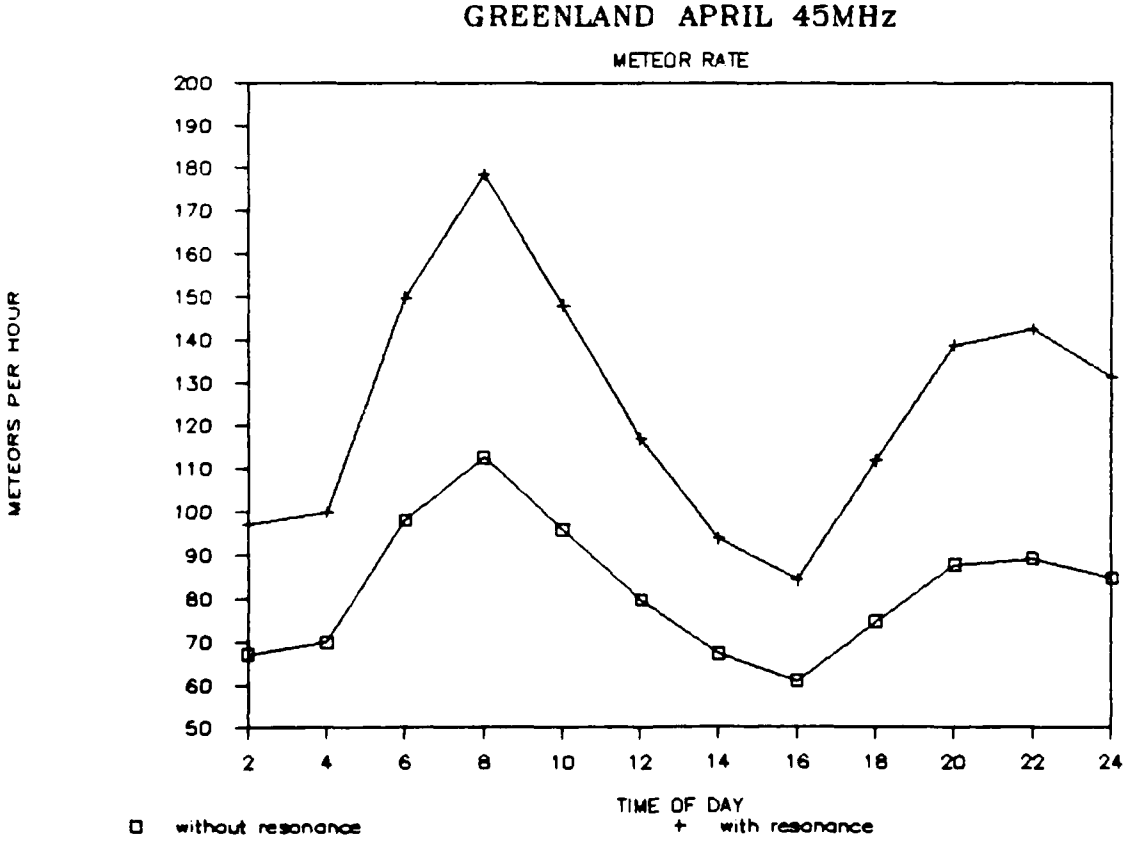

Figure 4-12. The Effect of Transverse Resonance on Model Results for the Greenland Link

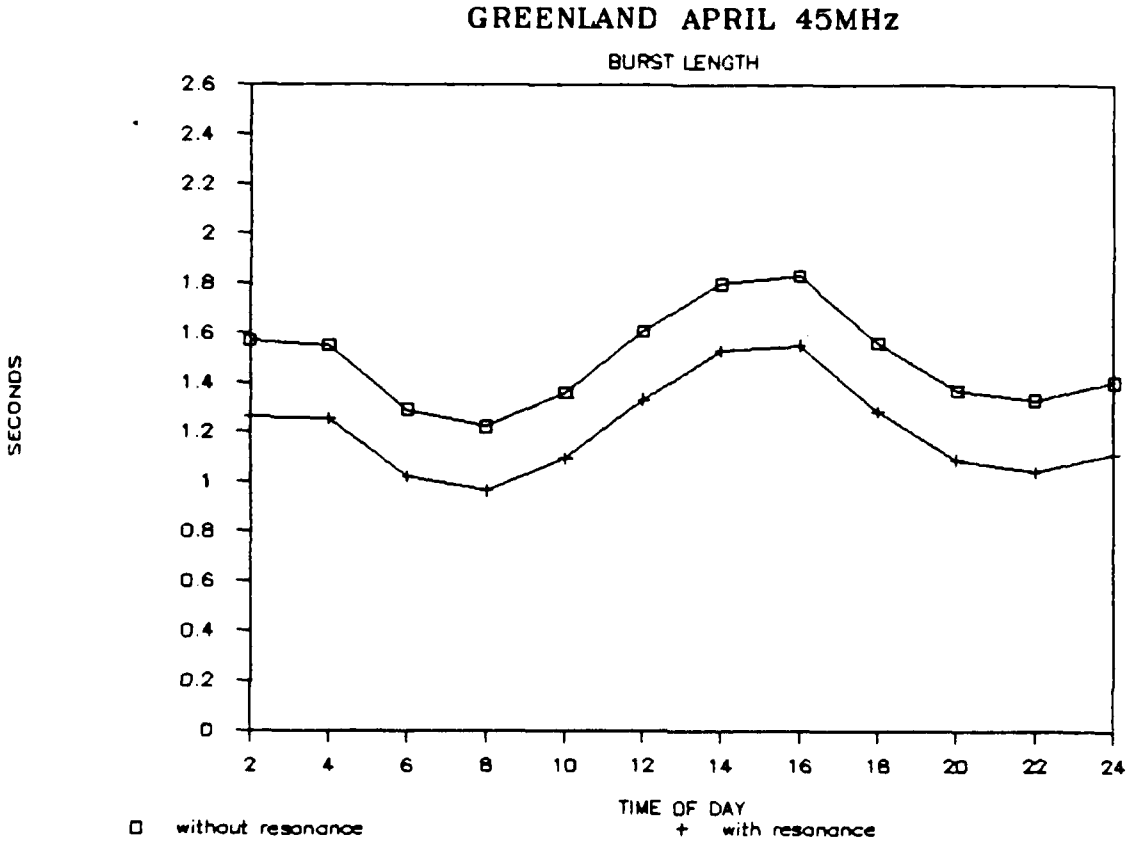

Figure 4-12. The Effect of Transverse Resonance on Model Results for the Greenland Link (Cont'd)

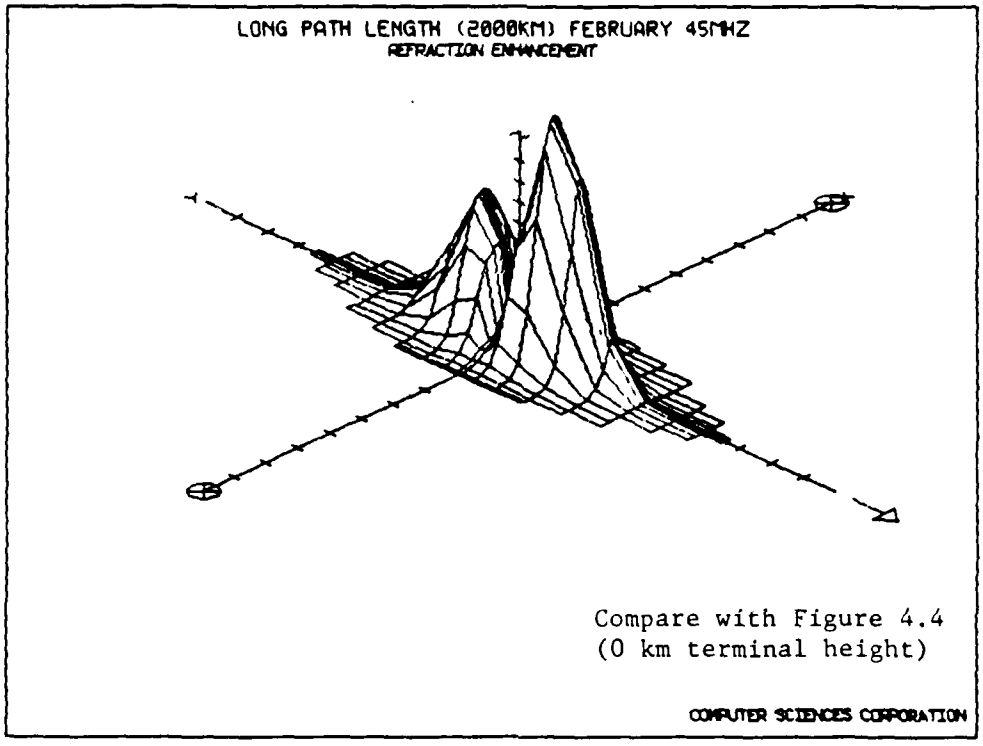

Figure 4-13. The Effect of Refraction on a Long East-West Link (2000 km)

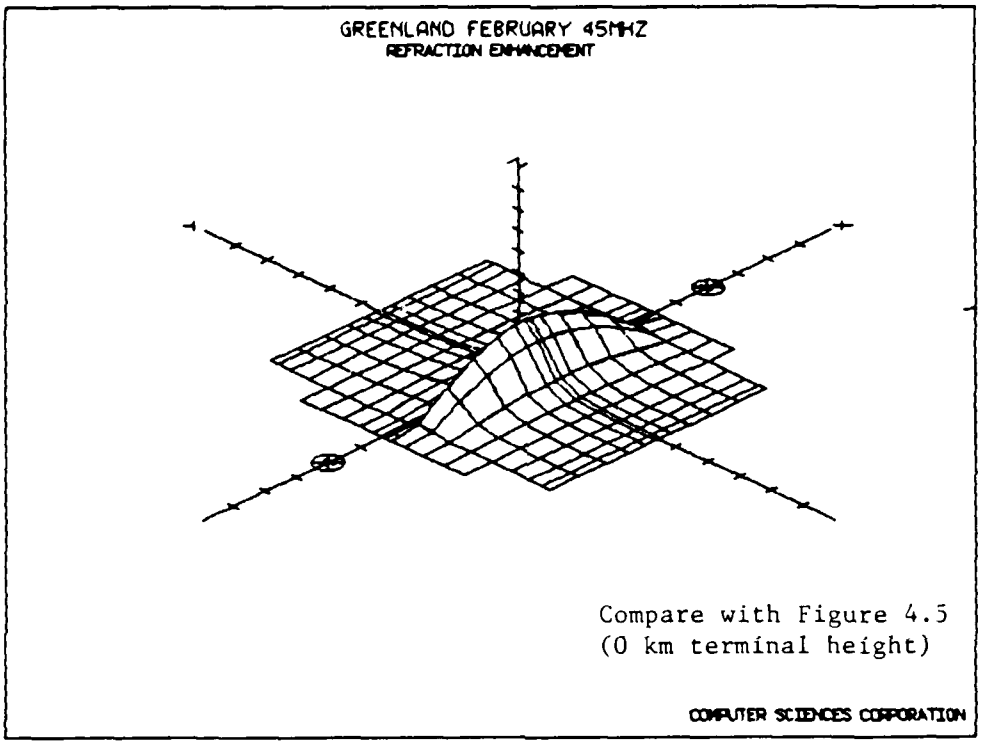

Figure 4-14. The Effect of Refraction on a Medium Length Link (1200 km)

4.7 SHOWER METEOR EFFECTS

Meteors can be divided into two categories: sporadic and shower. Sporadic meteors appear to be moving in mutually unrelated orbits and their arrivals are random. Meteors from a particular shower, however, move together in fairly well-defined orbits around the sun. Some showers appear to have meteoric particles distributed all along their orbit and therefore recur predictably year after year, whereas other showers have their particles concentrated in one portion of the orbit and the related showers may recur only after many years. Shower meteors make up only a small portion of the total number of meteors encountered during a year; however, when present, they can greatly influence performance on a meteor burst link.

The model now has the optional capability to handle all major meteor showers of both northern and southern hemispheres as shown in Table 4-1. Model results for the STC link with and without showers are shown in Figure 4-15. The differences are largely due to the Arietids shower. Model results with showers compare well to measurements; this will be covered in detail in the subtask 2 report to follow.

Table 4-1. The Major Meteor Showers

SHOWER	DATE OF MAX	DURATION (DAYS)	RELATIVE INTENSITY
QUADRANTIDS	JAN 03	5.0	2.1
ARIETIDS & Z-PERSEIDS	JUN 05	16.0	11.3
BETA-TAURIDS	JUN 30	12.0	2.7
PERSEIDS	AUG 12	15.0	2.1
LEONIDS	NOV 17	5.0	0.5
GEMINIDS	DEC 13	3.0	5.8
PUPPIDS	DEC 14	23.0	1.1
VELIDS	DEC 20	30.0	1.1
ETA-AQUARIDS	MAY 05	20.0	5.1
SAGGITARIDS & CAPRICORNIDS	JUN 12	60.0	2.4
DELTA-AQUARIDS	JUL 28	21.0	7.9
PISCES AUSTRALIDS	AUG 03	35.0	3.4
O-CETIDS	MAY 19	10.0	6.5
URSIDS	DEC 22	4.0	2.2
ORIONIDS	OCT 21	10.0	1.8
LYRIDS	APR 21	8.0	0.9

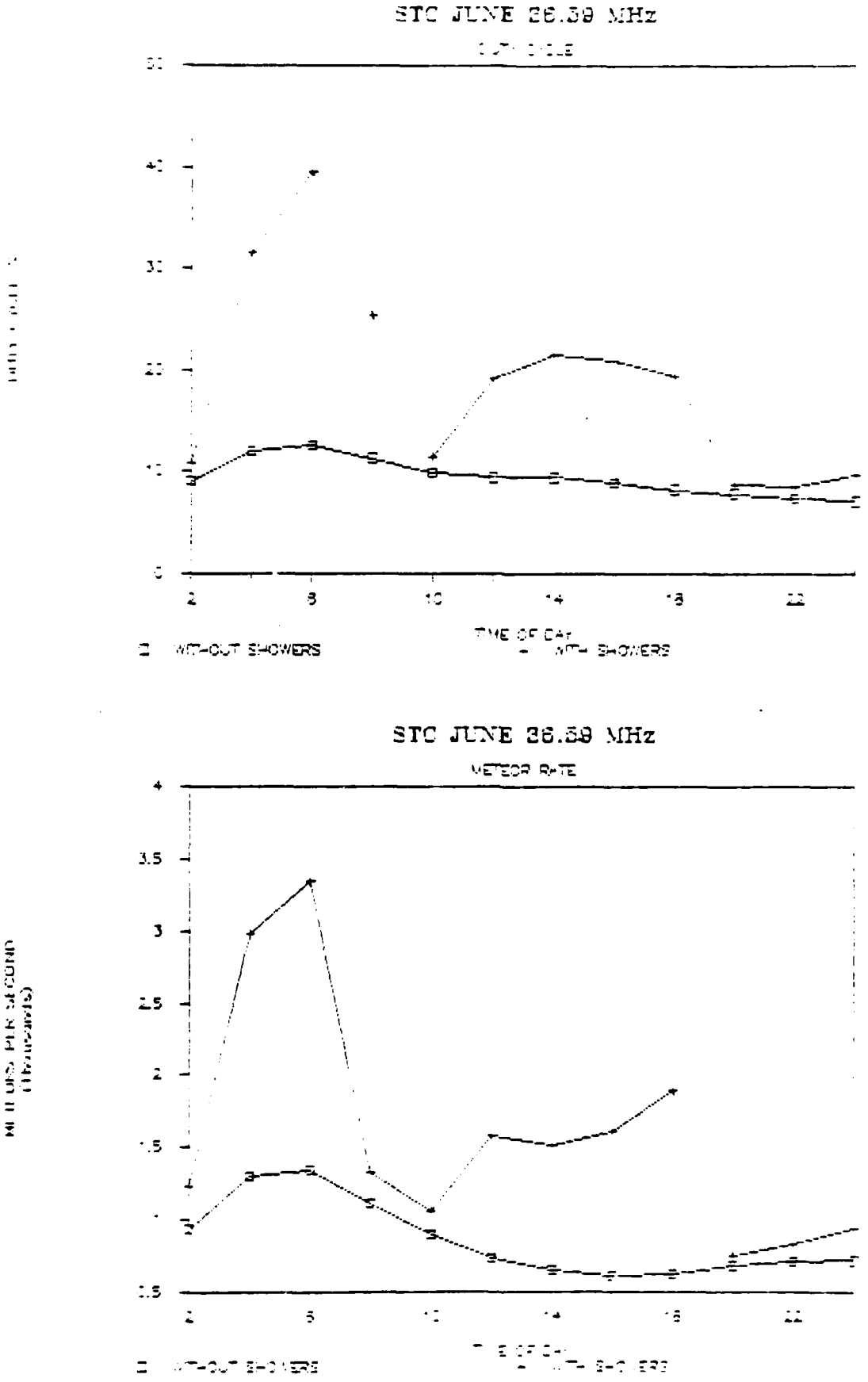

Figure 4-15. The Effects of Shower Meteors on the STC Link

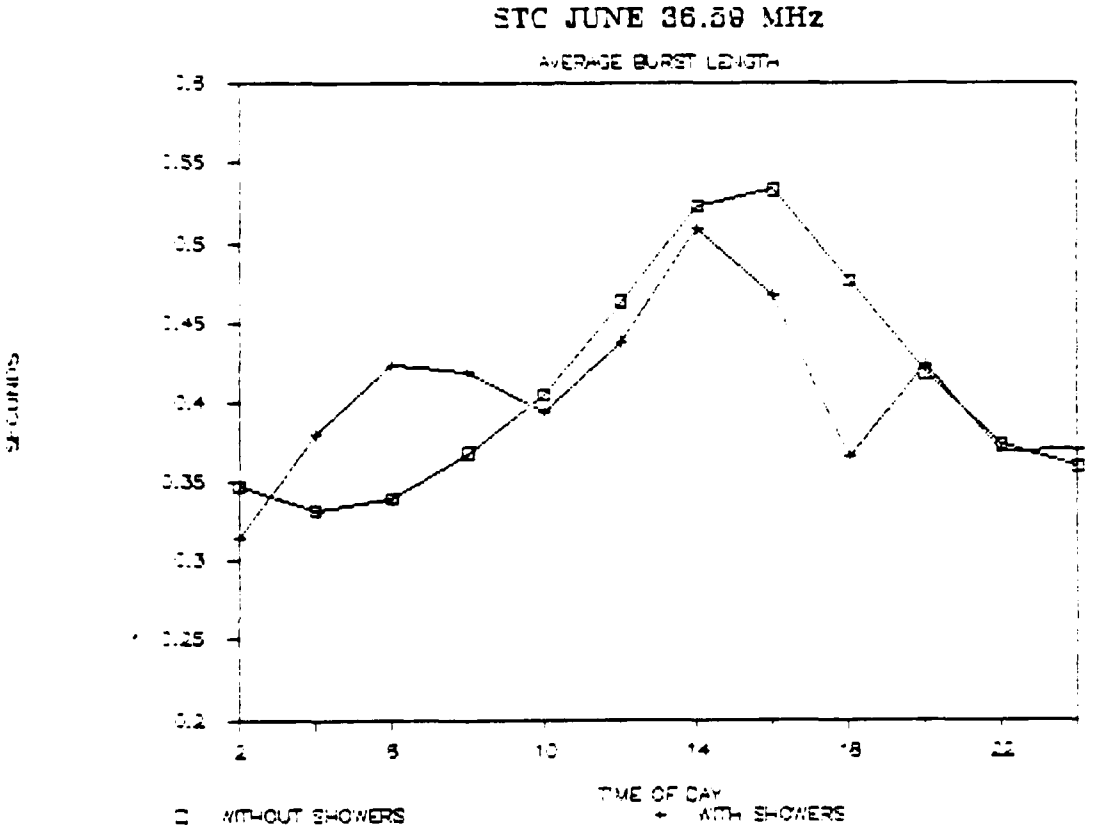

Figure 4-15. The Effects of Shower Meteors on the STC Link (Cont'd)

SECTION 5 - SUMMARY AND CONCLUSIONS

The previous section presented test results for each enhancement implemented in the CSC Meteor Burst Model under Task 7-85. To the extent possible those tests demonstrated the effect of a single enhancement with respect to the baseline results obtained with the preexisting model. This was the objective of subtask 1 for which this is the final report. In each case the results were qualitatively in accord with expectations so that there is a high confidence that the enhancements have been implemented as laid out in Reference 1.

In one instance, that of the explicit model of overdense bursts, the enhancement has certainly reduced agreement with measured results in respect of burst duration while improving agreement with burst rate. The purpose of Subtask 2 of this effort is to run the enhanced model against a variety of measured data. Based upon an analysis of those results, a one-time adjustment of constants in some of the ionospheric and meteor models will be made where justified. The prime candidate for such an adjustment is the model of diffusion constant versus altitude, which appears to be founded on an extrapolation rather than solid experimental data.

END

DTIC

4-86